Lithos 284–285 (2017) 327–346

Contents lists available at ScienceDirect

Lithos

journal homepage: www.elsevier.com/locate/lithos

Invited review article

Petrology and geochemistry of the orbicular granitoid of Caldera, northern Chile. Models and hypotheses on the formation of radial orbicular textures

Juan Díaz-Alvarado [a,*], Natalia Rodríguez [a], Carmen Rodríguez [b], Carlos Fernández [b], Ítalo Constanzo [a]

[a] Departamento de Geología, Universidad de Atacama, Copayapu 485, Copiapó, Chile
[b] Departamento de Ciencias de la Tierra, Universidad de Huelva, Campus del Carmen, 21071 Huelva, Spain

ARTICLE INFO

Article history:
Received 18 December 2016
Accepted 20 April 2017
Available online 27 April 2017

Keywords:
Columnar and equiaxial crystallization
Fractionation
Orbicule
Radial texture
Superheating
Undercooling

ABSTRACT

The orbicular granitoid of Caldera, located at the northern part of the Chilean Coastal Range, is a spectacular example of radial textures in orbicular structures. The orbicular body crops out as a 375 m^2 tabular to lensoidal intrusive sheet emplaced in the Lower Jurassic Relincho pluton. The orbicular structures are 3–7 cm in diameter ellipsoids hosted in a porphyritic matrix. The orbicules are comprised by a Qtz-dioritic core (3–5 cm in diameter) composed by Pl + Hbl + Qtz + Bt ± Kfs with equiaxial textures and a gabbroic shell (2–3 cm in diameter) characterized by feathery and radiate textures with a plagioclase + hornblende paragenesis. The radial shell crystals are rooted and orthogonally disposed in the irregular contact with the core. The radial shell, called here inner shell, is in contact with the granodioritic equiaxial interorbicular matrix through a 2–3 mm wide poikilitic band around the orbicule (outer shell). The outer shell and the matrix surrounding the orbicules are characterized by the presence of large hornblende and biotite oikocrystals that include fine-grained rounded plagioclase and magnetite. The oikocrystals of both the outer shell and the matrix have a circumferential arrangement around the orbicule, i.e. orthogonal to the radial inner shell. The coarse-grained granodioritic interorbicular matrix present pegmatitic domains with large acicular hornblende and K-feldspar megacrysts.

This work presents a review of the textural characteristics of the orbicules and a complete new mineral and whole-rock geochemical study of the different parts of the orbicular granitoid, together with thermobarometric and crystallographic data, and theoretical modeling of the crystallization and element partitioning processes. We propose a model for the formation of the orbicular radial textures consisting of several processes that are suggested to occur fast and consecutively: superheating, volatile exsolution, undercooling, geochemical fractionation and columnar and equiaxial crystallization.

According to the obtained results, the formation of the orbicular granitoid of Caldera may have initiated 1) during the generation of a magmatic fracture in the crystallization front of the Relincho pluton, where the water released by the host crystal mush was dissolved in the new batch of dioritic magma. 2) The high influx of water-rich liquids induced superheating conditions in the newly intruding magma that became a depolymerized liquid, where the only solid particules were the small irregular fragments of the host mush dragged from the fracture walls. 3) Volatile exsolution promoted crystallization under undercooling conditions. 4) Undercooling and nucleation around the core (cold germs) involved the physical and geochemical fractionation between two sub-systems: a gabbroic sub-system that comprises the solid paragénesis with a residual water-rich liquid and a granodioritic sub-system. 5) The orbicules, including core and inner shell, behaved as viscous bodies (crystals + residual liquid) floating in the granodioritic magma. 6) Higher undercooling rates occurred at the starting stage, close to the liquidus, promoting columnar crystallization around the cores and formation of the shells. Conversely, in the granodioritic matrix sub-system, equiaxial crystallization was promoted by low relative crystallization rates. 7) The rest of the crystallization process evolved later in the outer shell and the matrix, as suggested by the poikilitic textures observed in both sides of the orbicule contact, and under conditions close to the solidus of both sub-systems (shell and matrix). The water-rich residual liquid expelled during the orbicular shell crystallization was mingled with the partially crystallized matrix magma, generating the pegmatitic domains with large Kfs megacrysts.

* Corresponding author.
E-mail address: juan.diaza@uda.cl (J. Díaz-Alvarado).

http://dx.doi.org/10.1016/j.lithos.2017.04.017

Contents

1. Introduction . . . 328
1.1. Orbicular textures: facts and theories . . . 328
2. Geological setting . . . 329
3. Description of the orbicular body . . . 329
3.1. Dimensions and shape . . . 329
3.2. The contacts . . . 329
3.3. The host rocks . . . 329
3.4. Orbicules . . . 330
3.4.1. Orbicule core . . . 330
3.4.2. Orbicule shell . . . 331
3.5. Matrix . . . 333
4. Mineral geochemistry and crystallographic orientation . . . 333
4.1. Analytical techniques . . . 333
4.2. Mineral geochemistry . . . 333
4.2.1. Zone I, orbicule core . . . 333
4.2.2. Zone II, inner orbicule shell . . . 334
4.2.3. Zone III, outer orbicule shell-matrix contact . . . 335
4.2.4. Zone IV, matrix . . . 335
4.3. Thermobarometry results . . . 335
4.4. Study of the crystallographic preferred orientation (CPO) of quartz . . . 336
5. Whole rock geochemistry . . . 336
5.1. Analytical techniques . . . 336
5.2. Geochemistry results . . . 336
6. Crystallization models . . . 338
7. Discussion . . . 339
7.1. Where do orbicular granitoids occur? . . . 340
7.2. Why do radial orbicular textures occur? . . . 340
7.3. Building a model for generation of the orbicular granite of Caldera . . . 343
8. Conclusions . . . 344
Acknowledgements . . . 345
References . . . 345

1. Introduction

Radial textures found in orbicular granitoids are commonly meant to represent exotic examples of magmatic crystallization controlled by changing conditions of temperature, pressure, and/or H_20 content, rather than by the composition of the parental magma or the tectono-magmatic context where they are emplaced, mostly in small granitic apophyses included in large batholiths (e.g. Decrite et al., 2002; Elliston, 1984; Leveson, 1966; Moore and Lockwood, 1973; Piboule et al., 1989; Vernon, 1985). The most cited terms when discussing the petrogenesis of these orbicular structures are "superheating" and "undercooling", "supersaturation" or crystallization rates, with the significant presence of a volatile phase (e.g. Grosse et al., 2010; Vernon, 1985; Vigneresse, 2014). However, the conditions controlling the changes that promote orbicule crystallization has been better developed in alloy metallurgy (e.g. Browne, 2002; Carvalho et al., 2013; Thévoz, 1998), where the transition between columnar (skeletal or feathery textures) and equiaxial solidification is studied (Thévoz, 1998). Liquidus undercooling promotes oriented textures in granitic melts (London et al., 1989). As in pegmatites, the addition or exsolution of water and/or volátiles in orbicular granites promote changes in crystallization conditions (London, 2009; Vigneresse, 2014).

Orbicular granitoids have been described throughout the world in several localities and, albeit these structures are uncommon, they are associated to a wide variety of plutonic compositions (Elliston, 1984). Several authors, such as Sederholm (1928), Eskola (1938), Goodspeed (1942), Leveson (1966), Barrière et al. (1971), Barrière (1972), Moore and Lockwood (1973), Couturié (1973), Aguirre et al. (1976), Enz et al. (1979), Elliston (1984, 1985), Vernon (1985), Symes et al. (1987), Chauris et al. (1989), Owen (1991), Ort (1992), Sinclair and Richardson (1992), Decrite et al. (2002), Lahti (2005), Lindh and Näsström (2006), Tagiri et al. (2007), Abdallah et al. (2007), Kennan and Lorenc (2008), Grosse et al. (2010), among others, have contributed ideas about the genesis of orbicular structures.

Aguirre et al. (1976) first described the orbicular granitoid of Caldera (northern Chile), including macroscopic and petrographic descriptions. They also presented geochemical information mostly based on modal analyses. We here present a review of the textural characteristics of the orbicular granitoid of Caldera and a complete new mineral and whole-rock geochemical study of its constituent parts. We also propose a model for the formation of orbicular radial textures based on geochemical data, textural observations and theoretical models obtained by crystallization modeling.

1.1. Orbicular textures: facts and theories

Orbicular rocks are mostly found in the margins of intrusive plutonic complexes, as decametric to hectometric bodies (Decrite et al., 2002), associated with crystallization fronts, magma–host rock interaction areas or magma fractures (Abdallah et al., 2007; Fernández and Castro, 1999; Grosse et al., 2010). The orbicules are spheroidal to ellipsoidal structures composed by a core and one or several rings of typical granitic minerals (shell), which show radial and/or concentric textures (e.g. Elliston, 1984). The orbicular cores can be made of country rock fragments (mostly granitoids), mineral aggregates or individual crystals from the orbicular magma or the host rock (Decrite et al., 2002; Elliston, 1984; Grosse et al., 2010). The shell may present two main configurations: 1) rhythmic and concentric growth around the core of ferromagnesian and quartz-feldspathic minerals, or 2) radial growth of different mineralogies with feathery or spherulitic textures rooted in the presumably solid core (Aguirre et al., 1976; Elliston, 1984; Lindh and Näsström, 2006; Tagiri et al., 2007). Both shell structures give the orbicule (core and shell) the spheroidal or ellipsoidal shape. The orbicules are hosted by an inter-orbicular matrix, which is generally described as an equiaxial granitic rock with varied compositions. If the orbicule and its matrix crystallize from different mingled liquids, which is an acceptable hypothesis if we consider the ubiquitous presence of ductilely deformed contacts between the orbicules, and between them and xenoliths present in the orbicular granitoid, surface tension will tend to minimize the surface contact area between both liquids, therefore yielding spheres (Ballhaus et al., 2015). The frequent presence of pegmatite textures in the inter-orbicular matrix is indicative of volatile phase activity during the crystallization process of the orbicular magma (Aguirre et al., 1976; Elliston, 1984; Grosse et al., 2010; Sederholm, 1928).

The diversity of orbicular textures (see texture definitions in Lofgren, 1974), summarized in concentric rhythmic and radial, and the high geochemical variability of the orbicular granitoids have hampered to achieve a single petrogenetic hypothesis about the formation of these textures. Elliston (1984), in a review of orbicular textures, proposed that orbicular magmas must be similar to a concentrated macromolecular gel of mixed hydrosilicates. In addition, proposals on the formation of orbicular textures can be mainly summarized in the following three hypotheses: 1) a rapid diffusion process that controlled crystallization of the different elements composing the magma (Meyer and Altherr, 1991; Palmer et al., 1967), 2) mingling of two immiscible magmas (Barrière, 1972) or a hydrous magma where a fluid phase is exsolved, which is replaced during cooling and crystallization by an anhydrous paragenesis with magmatic textures (Ballhaus et al., 2015), and 3) atypical radial and tangential crystallization due to the absence of crystallization nuclei, which are resorbed previously during superheating processes (Aguirre et al., 1976; Grosse et al., 2010; Lindh and Näsström, 2006; Piboule et al., 1989; Vernon, 1985).

The hypotheses about columnar or dendritic crystallization are based on delayed nucleation or on undercooling, and relate the orbicular textures to low nucleation rates and high growth rates (Lofgren, 1974; London, 2009; Spillar and Dolejs, 2013). However, the plutonic context where this type of textures are described (e.g. Vernon, 1985), almost excludes the possibility that crystallization was triggered by a sudden temperature variation ($\Delta T = 200$–300 °C or 50–90 °C depending on starting materials: Lofgren, 1974), which is argued for the crystallization of spherulitic or dendritic textures in submarine or lunar basalts (Lofgren, 1974; Waters et al., 2015). Therefore, the role of the volatile phase seems essential to generate superheating and dissolution of proto-nuclei (Vernon, 1985), and undercooling and high growth rates for the appearance of tabular crystals at small ΔT, and skeletal crystals, dendrites, and spherulites with increasing ΔT, which is favored by a small diffusion coefficient/growth rate ratio (Keith and Padden, 1963; Lofgren, 1974). A critical pressure drop may be also considered as an effective mechanism to induce superheating and the subsequent undercooling during the volatile phase exsolution (e.g. Hammer and Rutherford, 2002; Waters et al., 2015).

The crystallization of orbicular granitoids may have its experimental parallel in metallurgy in the transition between equiaxial and columnar solidification in steel (Carvalho et al., 2013; Thévoz, 1998). Columnar solidification proceeds unidirectionally (dendritic), and is similar to the feathery textures of Kfs or Pl + Hbl in orbicular shells (e.g. Aguirre et al., 1976). The transition to an equiaxial crystallization produces intergrowth crystals similar to orbicular matrix textures. The transition between the two mechanisms of crystal growth is a complex process, but is mainly influenced by the cooling rate and associated with melt polymerization and increase in nucleation density (Spillar and Dolejs, 2013; Thévoz, 1998).

2. Geological setting

The orbicular tonalite is located in the Atacama region, northern Chile, 11 km north of the city of Caldera. It is included in the Relincho pluton that has a batholitic size and ellipsoidal shape, with a long-axis length of 23 km. Both the Relincho pluton and the orbicular body are cut by diabase dykes (Godoy and Lara, 1999). The Relincho pluton intrudes the Las Tórtolas Formation (e.g., Bell, 1982; Fuentes et al., 2016). The pluton presents a great compositional variety, including gabbros, Qtz-diorites, tonalites varying in grain size and occasionally showing magmatic foliation and ductile deformation, granodiorites and granites (Godoy and Lara, 1999). An age range between 193.6 ± 0.6 and 181 ± 5.4 Ma has been determined for the Relincho pluton (Brook et al., 1986; Dallmeyer et al., 1996), while the orbicular intrusive body yielded an age of 182 ± 6 Ma (Farrar et al., 1970). Therefore, the orbicular tonalite of Caldera and its hosting Relincho pluton are virtually coeval.

Magmatism in northern Chile during the Lower Jurassic to Cretaceous coincides with an extensional tectonic event along the convergent margin of South America (Charrier et al., 2007) (Fig. 1a). Mainly, it corresponds to the development of a magmatic arc along the Coastal Range (i.e., the Coastal Range batholith), parallel to the continental margin. The re-activation of subduction, that remained inactive for a period lasting about 40–50 Ma, is probably the main cause of the development of extensional tectonic conditions and the intense magmatic activity, giving place to the Coastal Range batholith, contemporary with arc and back-arc volcanism (Charrier et al., 2007; Mpodozis and Ramos, 2008).

3. Description of the orbicular body

3.1. Dimensions and shape

The orbicular granitoid crops out as a 15 m thick tabular to lensoidal intrusive body, enclosed by the Relincho pluton (Fig. 1b). It can be discontinuously followed along the shore line for approximately 25 m, thus covering a total area of approximately 375 m^2 (Aguirre et al., 1976) (Fig. 1c). The body is characterized by the presence of spheroidal to ellipsoidal orbicules, which consist of a Qtz-dioritic core and a gabbroic shell. These orbicules are hosted in a medium- to coarse-grained porphyritic granodiorite matrix, where K-feldspar phenocrysts, varying in size from 4 to 9 cm, are included.

3.2. The contacts

The contacts between the orbicular intrusive body and the country tonalitic rocks can be observed along its western and eastern margins. The contacts are lobulated, showing 2–3 cm wide dark bands with Pl-Hbl radiate textures, similar to the orbicular shells, and do not alter or cut the orbicules. The eastern contact is disposed in a NE-SW orientation (Figs. 1c, 2a). In this area, an internal curved dark band can be observed within the orbicular body (Fig. 2b). The shape of the orbicules is adapted to the lobulated trace of the band, and they are not cut by it. The western contact is observed in the intertidal zone and has an N-S orientation, also showing a narrow dark band of a few centimeters (Fig. 2c). In the host tonalitic rocks, close to the contact, small and poorly developed orbicules are observed. Some orbicules are cut and slightly displaced by late fractures that affect and crosscut the entire intrusive body.

3.3. The host rocks

The rock that host the orbicular granitoid is a medium to coarse grained tonalite (2–4 mm) composed by Pl, Qtz, Hbl, Bt and Cpx as resorbed crystals included in Hbl (abbreviations by Kretz, 1983). The host tonalite presents holocrystalline, equigranular and hypidiomorphic textures. Pl is present as normally or oscillatory zoned coarse grains and Cpx irregular cores are included in Hbl aggregates. The host tonalites are macroscopically similar to the orbicular cores (Fig. 2a and c).

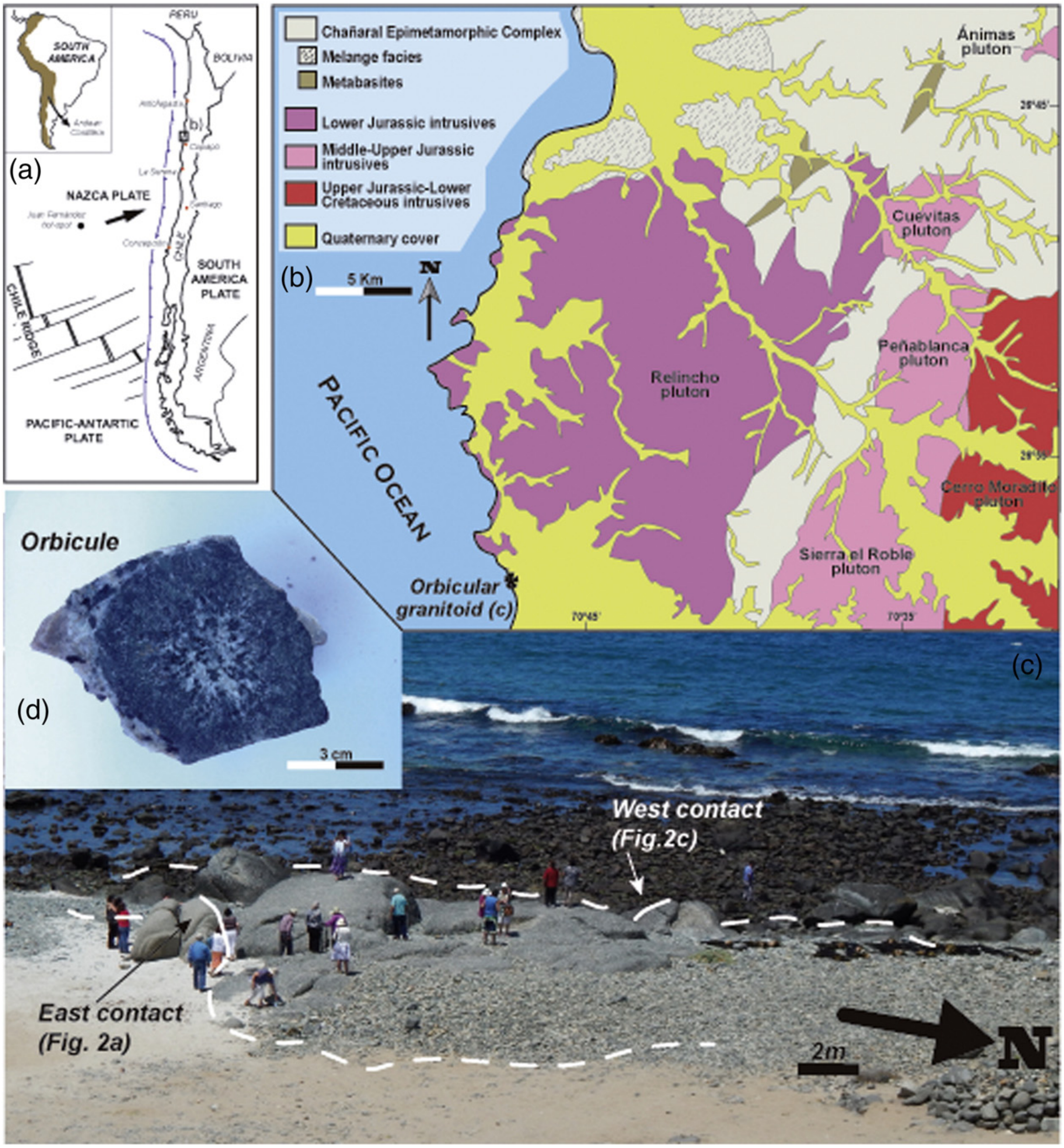

Fig. 1. (a) Plate configuration of the western margin of South America (modified from Charrier et al., 2007). (b) Geological sketch showing the configuration of the intrusive units that comprise de Coastal Range batholith and its Paleozoic metasedimentary host-rocks (modified from Godoy and Lara, 1999). The location of the orbicular granitoid of Caldera is given by an asterisk. (c) General view of the orbicular body outcrop (use people as scale). (d) Hand sample of an orbicule showing the core, shell and part of the host matrix.

3.4. Orbicules

The orbicules are mainly composed of a well-defined light-gray core and a dark radial shell. However, a few orbicules show a concentric disposition of quartz-feldespathic and mafic minerals (Fig. 2d). The morphology of the orbicules is predominantly spheroidal to ellipsoidal, with some minor exceptions showing "heart" or triangular shapes with rounded corners (Fig. 2e). Besides, a few large host rock xenoliths, macroscopically similar to the cores of the orbicules, but without the radial mafic shell, are also present (Fig. 2f). The external shape and size of the orbicules mostly mimics those of the cores, while the orbicular shells present a constant width (2–3 cm) regardless of the core size (Fig. 2e and f). The shape preferred orientation (SPO) fabric of the orbicular body, calculated in three orthogonal sections using Ellipsoid 2003 (Launeau and Robin, 2005; Robin, 2002), results in a nearly spherical prolate ellipsoid, with values of 1.086, 1.060 and 1.025 for X/Z, X/Y and Y/Z ratios respectively (Supplementary material, Annex 1). The orientation of the X axis is N211° E, dipping 36° SW.

On average, the orbicules make up around 65% in volume of the orbicular body, with an average size of 3 to 4 cm for the short axis and 5 to 7 cm for the long axis.

3.4.1. Orbicule core

The orbicule cores (3–5 cm in diameter) have equiaxial textures typical of the plutonic rocks and an apparently rounded shape. However, in detail, the contact with the shell has an irregular shape (Fig. 3). The orbicular core is characterized by its light-gray color, with an average grain size that varies from 0.8 to 2.0 mm. It presents holocrystalline,

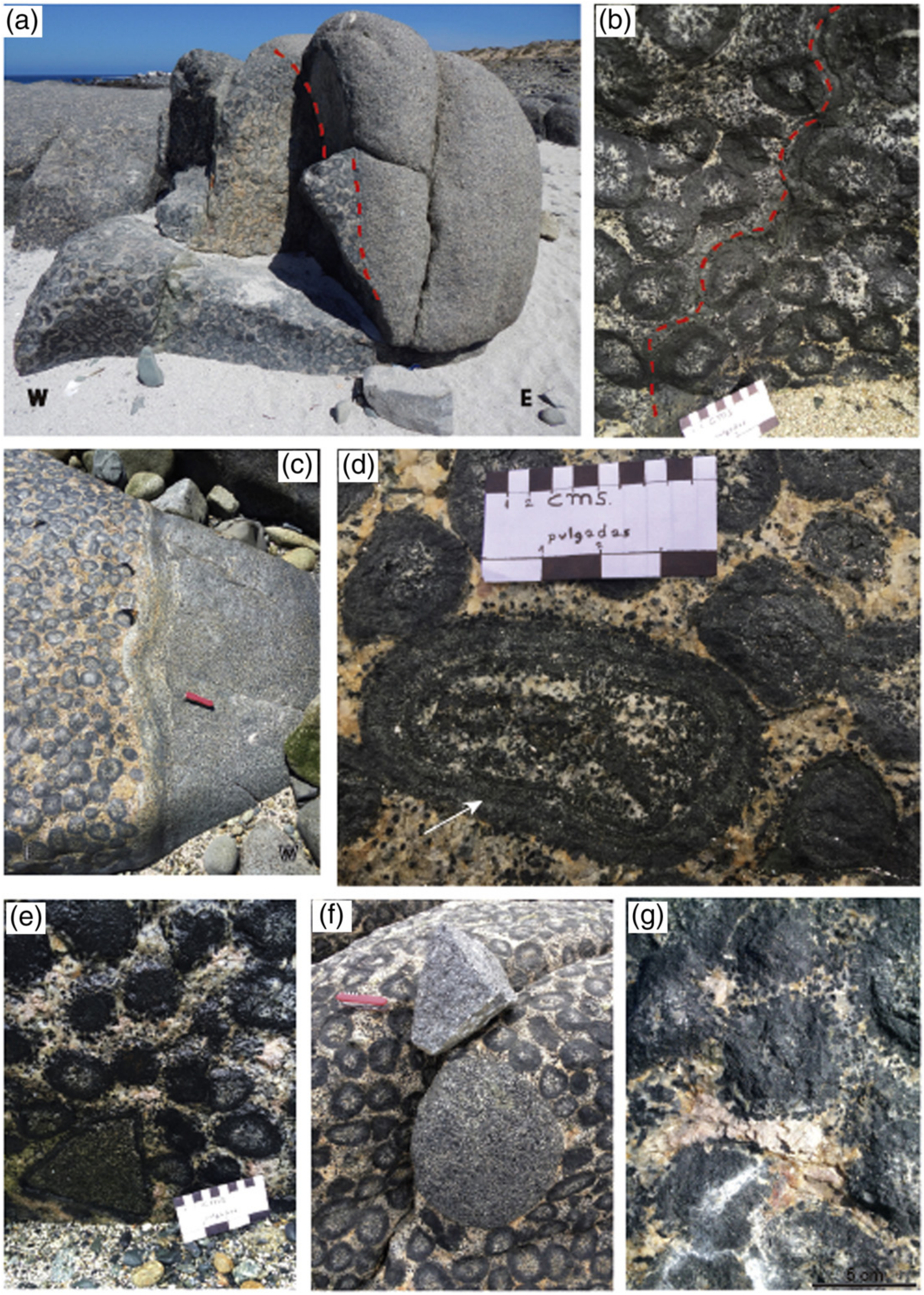

Fig. 2. Field photographs of some outstanding features of the orbicular granitoid. (a) The contact between the orbicular body and the host Relincho pluton is a sharp 2–3 cm wide comb layering band. (b) Internally, the orbicular granitoid presents some of these contact bands. The shape of the orbicules is adapted to the principal and internal contacts. (c) The west contact along the shoreline shows a narrow comb layering band. (d) Most of the orbicules consist of spherical cores with a single radial shell. However, some of them show internal contacts in the Hbl + Pl + Cpx shell (white arrow), or (e) triangular shaped cores. "Black orbicules" are common depending on the outcrop section. (f) Large host tonalite enclaves within the orbicular body. A tonalite sample from the Relincho pluton outside the orbicular body is shown for comparison. (g) A large matrix Kfs megacryst flattened between two orbicules.

phaneritic and equigranular textures and is composed of Pl, Hbl, Qtz, Bt, and Chl (as alteration mineral), with minor Kfs (Fig. 3a). The contact between the core and the shell of the orbicule is given by the root of large feathery Hbl and Pl crystal aggregates that grow radially outwards.

3.4.2. Orbicule shell

The orbicular shells (2–3 cm in diameter) present two zones, inner and outer, with a similar mineral assemblage comprised by Pl, Hbl, Cpx, Mag and interstitial Qtz (Fig. 3). The inner shell shows a radial texture around the core. Textural terms used for such a type of crystal

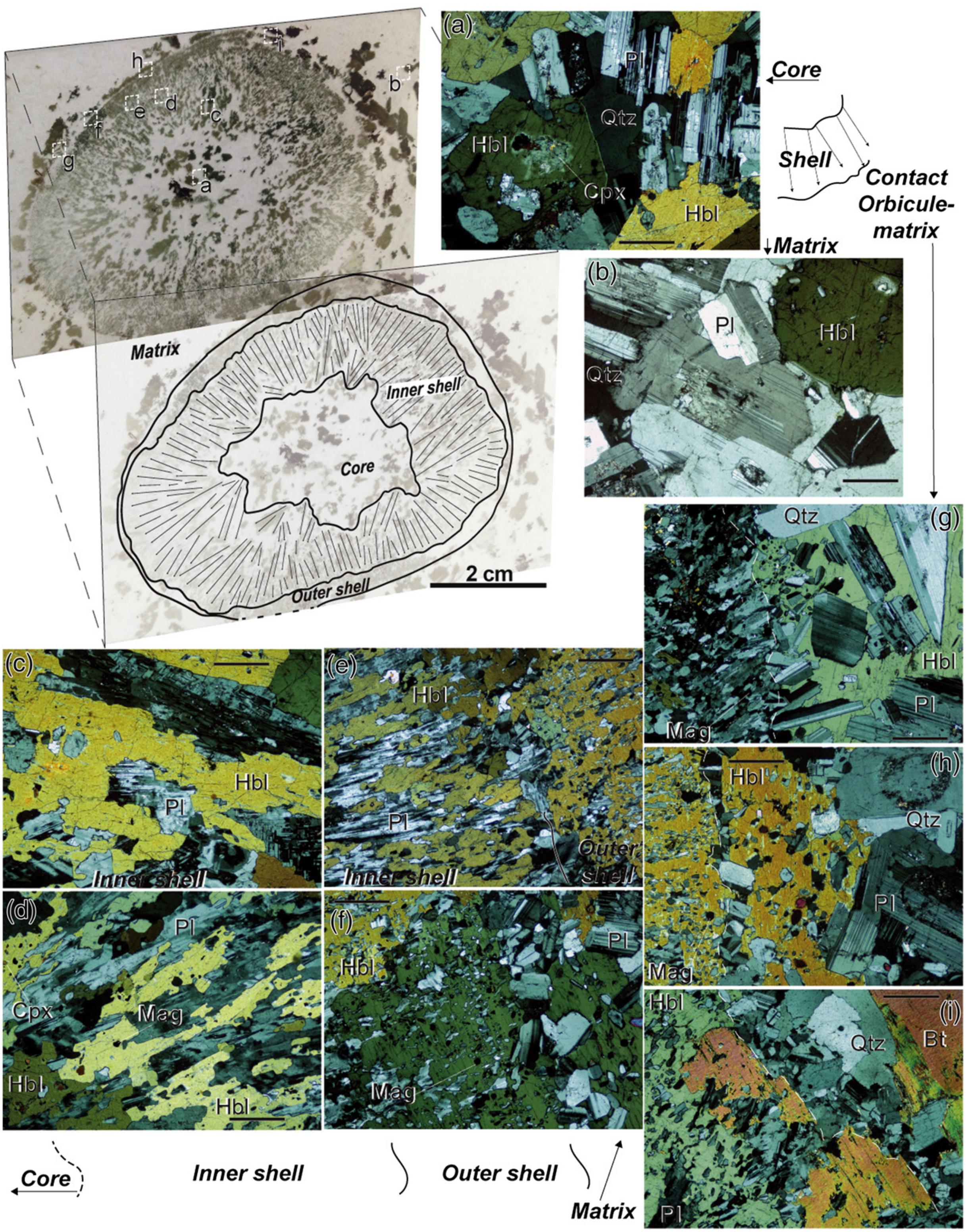

Fig. 3. Plane-polarized image of an orbicule and corresponding sketch, showing the different orbicule zones and the location of cross-polarized microphotographs (a) to (i). Black arrows in sketch indicate the maximum elongation of the shell Hbl + Pl crystals. Black scale bars in the microphotographs are 500 μm. (a) Equiaxial textures in the coarse-grained equigranular core. Reserved Cpx appears in the Hbl cores, while the scarce Qtz occupies interstitial spaces. (b) The granodioritic matrix has similar textures to the core with Pl + Qtz + Hbl + Bt + Kfs mineralogy and equiaxial crystallization. (c) (d) The orbicular inner shell has large feathery Hbl and Pl crystals rooted in the core contacts. Where the contact shows a planar limit, the Hbl + Pl shell crystals are orthogonal to it (see orbicular sketch). Cpx appears as reserved or ghost crystals in the Hbl cores. (e) (f) Radiate textures observed in the inner shell end at the outer shell, where large Hbl oikocrystals are arranged parallel to the shell-matrix contact. Rounded Pl and Mag are included in Hbl oikocrysts. (g) (h) (i) The orbicule-matrix contact shows a fine-grained narrow band (white dashed line) with mainly Pl and Mag crystals. Large matrix Hbl and Bt crystals are disposed parallel to the contact, and they extend and include the small crystals of the contact band. Both Bt and Hbl are parallel to the outer shell oikocrysts.

morphologies are fan or plumose spherulitic textures (Keith and Padden, 1963; Lofgren, 1974). Large feather-like Hbl and Pl crystal aggregates (between 0.5 and 1 cm long) are rooted in engulfed areas of the irregular contact, while in more planar contact zones the spherulitic Hbl and Pl crystals grow orthogonal to the contact (Fig. 3c, d and e). Pl and Hbl present euhedral to subhedral elongated crystals and crystal patches (compositionally distinguishable areas not concentrically arranged). Cpx, showing resorption boundaries, is found in the core of large feathery and spherulitic Hbl crystals. The inner shell ends in a narrow band (2–3 mm) formed by large Hbl oikocrystals (up to 0.5 cm long) that include rounded Pl and Mag and are disposed parallel to the orbicule-matrix contact. This area is here called outer shell and puts into contact the radial inner shell with the equiaxial inter-orbicular matrix (Fig. 3e and f). The traces of the cleavage planes of the Hbl oikocrysts are parallel to the contact between the outer shell and matrix. These Hbl crystals are identical to those of the matrix close to the contact (Fig. 3f).

3.5. Matrix

The contact between the outer shell and the matrix presents small Pl and Mag crystals. Large Hbl crystals occupy interstitial spaces between coarse-grained Pl in the matrix, but also grow over this small-grained narrow band (Fig. 3g and h). Where Bt is abundant in the matrix, it is also present as oikocrysts in the outer shell and the matrix around the orbicules, where, as the Hbl oikocrysts, it is arranged parallel to the contact trace (Fig. 3i).

The matrix is a light-gray granodiorite with a medium to coarse grain size (5 mm to 8 cm). It consists of Pl, Qtz, Kfs, Hbl, Bt and Ep and Chl as alteration minerals. The matrix presents holocrystalline, phaneritic, porphyritic and pegmatitic textures (Fig. 3b). The pegmatitic domains show large Kfs crystals (4 to 8 cm) and large Hbl acicular crystals. It is remarkable the presence of plastically deformed Kfs megacrysts, located between two or more orbicules (Fig. 2g).

4. Mineral geochemistry and crystallographic orientation

4.1. Analytical techniques

Electron microprobe analyses of the orbicular and matrix minerals were obtained with a JEOL JXA-8200 SuperProbe at the University of Huelva. A combination of silicates and oxides were used for calibration.

One thin section of a selected orbicule was polished with colloidal silica (0.02 □m) and analyzed for EBSD (electron back-scattered diffraction) at the High-Resolution Scanning Electron Microscopy (HRSEM), AURIGA (FIB-FESEM) from Carl Zeiss SMT, at the CIC, University of Granada (Spain). The acceleration voltage was of 10.00 kV and the specimen tilt of 70°. Data analysis and microstructure imaging was done with Aztec 3.0 and post-processing software of Oxford Instruments.

4.2. Mineral geochemistry

The orbicules and the matrix where they are included have been divided in four zones regarding the mineralogical and textural characteristics described above (Table 1, Fig. 4).

4.2.1. Zone I, orbicule core

The core is a medium- to coarse-grained plutonic rock with equiaxial texture (Fig. 4a, b). The dominant mineral assemblage of the orbicule core is formed by Pl + Hbl + Qtz with subordinated Cpx, Kfs, Ilm, ±Mag (Fig. 4b). Plagioclase is present as zoned, euhedral crystals of bytownite (70–90 mol% An) with labradorite external rims (65 mol% An) (Fig. 4b, Table 1). Plagioclase cores show patches of different % An, with minor Kfs and Qtz. Hornblende presents euhedral to subhedral crystals (Mg# = 0.56–0.60, see the comparison between the mineral

Table 1
Selected geochemistry results for the mineral paragenesis observed in the orbicular zones.

Orbicular zone	Core						Inner shell							Outer shell - contact					Matrix					
Mineral	Hbl	Pl1[1]	Pl2[2]	Cpx	Kfs	Mag	Hbl	Pl1	Pl2	Cpx	Kfs	Mag	Bt	Hbl	Pl1	Pl2	Mag	Bt	Hbl	Pl1	Pl2	Kfs	Mag	Bt
SiO_2	45,75	48,38	54,54	52,13	63,92	2,57	46,22	48,63	52,45	52,45	63,28	0,03	36,37	43,69	49,21	55,80	0,05	35,77	46,04	51,97	54,44	63,25	0,03	36,17
TiO_2	1,30	0,01	0,02	0,12	0,06	0,02	1,07	–	0,07	0,05	0,00	0,10	3,08	1,28	0,04	–	0,06	3,15	1,75	–	–	0,00	48,97	2,65
Al_2O_3	8,06	32,94	28,95	0,81	18,68	0,01	7,84	32,72	29,05	0,49	18,82	0,18	14,87	9,20	32,49	27,91	0,16	15,15	8,34	30,77	29,34	18,86	–	15,19
FeO	15,69	0,16	0,22	9,25	0,03	70,84	16,68	0,14	0,15	9,24	0,04	89,88	17,98	17,93	0,21	0,19	91,74	20,39	14,96	0,17	0,12	–	47,58	20,57
MgO	12,48	0,01	–	13,10	0,00	0,94	11,76	–	0,01	12,93	–	0,03	12,29	10,28	–	0,00	0,01	10,77	13,27	–	0,01	0,01	0,07	11,59
MnO	0,22	0,01	–	0,40	–	0,08	0,38	–	0,01	0,38	–	0,12	0,19	0,38	–	0,01	0,11	0,18	0,31	–	–	0,04	3,44	0,12
CaO	11,61	15,45	10,60	23,08	–	0,29	11,68	15,22	10,87	23,41	0,01	0,07	–	11,77	14,54	9,22	0,03	0,00	11,33	12,61	11,04	0,01	0,01	0,03
Na_2O	1,10	2,70	5,28	0,29	0,41	0,03	0,88	2,72	5,10	0,29	0,68	–	0,08	0,98	3,08	5,98	0,03	0,07	1,19	4,32	5,18	0,90	0,02	0,08
K_2O	0,95	0,05	0,19	0,01	16,62	0,01	0,82	0,05	0,15	0,01	15,99	–	9,56	1,19	0,06	0,20	–	9,69	0,99	0,08	0,17	15,77	–	9,52
P_2O_5	0,03	0,00	–	–	–	0,01	0,00	0,03	–	0,00	0,03	0,03	0,02	0,01	0,02	0,03	0,01	0,00	–	–	0,03	–	0,02	-
SO_3	0,02	0,01	0,02	0,00	0,01	0,28	0,03	–	–	–	0,00	–	0,04	–	0,03	0,04	–	0,23	0,01	0,01	0,00	–	0,01	0,06
Cr_2O_3	0,06	0,02	–	0,04	0,01	0,02	0,06	0,13	0,04	0,03	–	0,29	–	–	–	–	0,16	0,02	–	0,02	0,03	0,02	0,23	0,11
NiO	0,00	0,04	–	–	–	0,16	0,01	–	0,02	–	–	0,01	0,08	0,07	0,04	–	–	0,04	0,05	0,00	–	–	–	0,01
F	0,12	0,08	0,10	–	0,21	–	–	–	–	–	–	–	0,17	0,02	–	–	0,04	0,04	0,30	0,05	–	0,00	–	0,30
SrO	–	0,01	0,03	–	–	0,05	–	0,07	0,03	–	–	–	–	–	–	0,05	0,00	–	–	0,05	0,06	–	0,02	–
BaO	–	0,03	0,08	–	0,12	0,06	0,12	–	0,04	–	0,27	–	0,39	–	0,01	0,12	–	0,04	0,07	–	–	0,32	0,07	0,15
Total	97,32	99,85	99,98	99,23	99,98	75,37	97,55	99,71	97,98	99,29	99,13	90,75	95,03	96,79	99,73	99,53	92,39	95,44	98,48	100,02	100,40	99,16	100,46	96,41

*Pl[1]: Ca-rich zone or patch.
*Pl[2]: Ca-poor zone or patch.

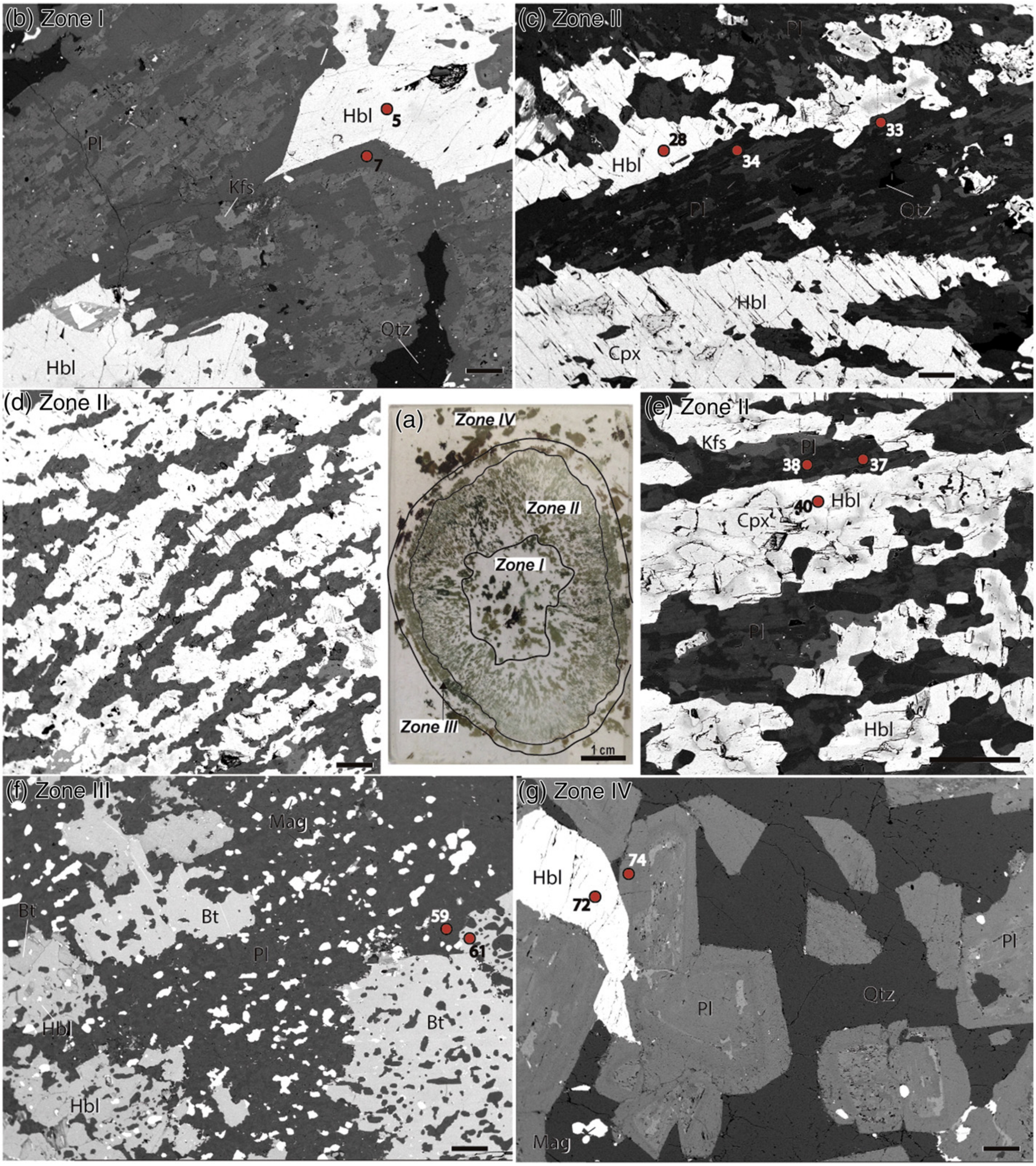

Fig. 4. Back-scattered Electron (BSE) images of the different zones of the orbicular body. Location of the Hbl and Pl points analyzed for the thermobarometric study are shown. Scale bars are 100 μm. (a) Sketch of the orbicule and its different zones. (b) Zone I, orbicular core. (c) (d) (e) Zone II, inner orbicular shell. (f) Zone III, outer shell and orbicule-matrix contact. (g) Zone IV, orbicular matrix.

geochemistry per zone in Fig. 5). Occasionally, Cpx (Mg# = 0.72) appears as resorbed crystals in the Hbl core. The limit of the orbicule core is marked by the presence of acicular radial and feather-like large Hbl crystals from the shell (Zone II) (Figs. 3 and 4a).

4.2.2. Zone II, inner orbicule shell

The inner shell mainly consists of medium to coarse-grained elongated Pl + Hbl crystals with subordinated Cpx, Qtz, Kfs and Mag (Fig. 4a–d). Pl patches are elongated parallel to the Hbl crystals

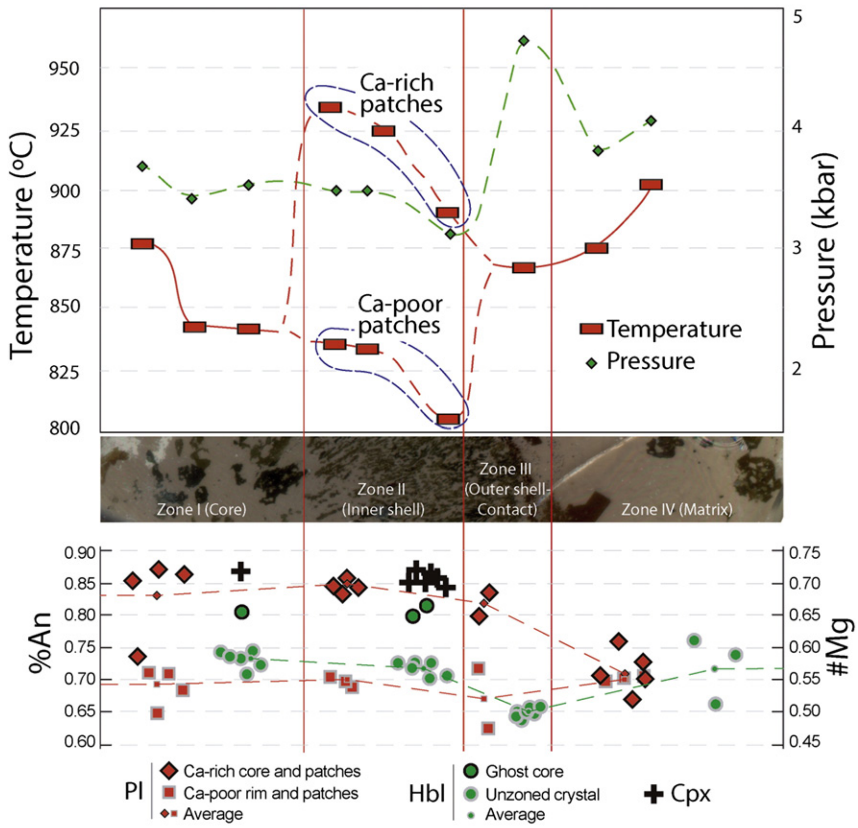

Fig. 5. Temperature and pressure vs. orbicule zone diagram, showing the thermobarometric results according to the Pl-Hbl locations. At the bottom, the % An in Pl and #Mg in Hbl and Cpx show the geochemical variations across the different orbicular zones.

(Fig. 4d, e). Compositionally, the Pl crystals are bytownite (70–86 mol% An), with minor interstitial Qtz and Kfs. Cpx (Mg# = 0.69–0.72) forms resorbed crystals included in Mg-Hbl (Mg# = 0.55–0.58) (Fig. 4c, d, Table 1). Inner shell mineral paragenesis show similar compositions from the contact with the core to the outer shell (Fig. 5).

4.2.3. Zone III, outer orbicule shell-matrix contact

The contact between the orbicule and its matrix is characterized by the transition between the orthogonal arrangement of the Pl + Hbl assemblage of the inner orbicular shell, and the Bt and Hbl crystals of the matrix, which are aligned according to the spheroidal shape of the orbicule (Fig. 4f). The contact is characterized by an assembly of Pl and Mag crystals, which are almost absent in the shell, included in Pl, Hbl, and Bt crystals. Plagioclase shows compositional patches of bytownite-labradorite (63–84 mol% An) and is present as inclusions in Bt and Hbl large crystals. Subhedral Hbl (Mg# = 0.49–0.51) and Bt (Mg# = 0.46–0.50) oikocrysts conform a narrow band in the outer shell and around the orbicule with abundant inclusions of Pl and Mag (Fig. 4f, Table 1).

4.2.4. Zone IV, matrix

The matrix is a coarse-grained granodioritic rock with equiaxial texture (Fig. 4g) and pegmatitic domains. The dominant mineral assemblage in the matrix is formed by Pl + Qtz + Kfs + Bt + Hbl with subordinated Ilm ± Mag. Plagioclase is present as euhedral crystals with concentric zoning of bytownite cores (70–73 mol% An) and labradorite external rims (67 mol% An) (Fig. 4g, Table 1). Hornblende (Mg# = 0.52–0.60) and Bt (Mg# = 0.50) are present as euhedral crystals.

4.3. Thermobarometry results

Thermobarometry techniques have been applied to ascertain the pressure and temperature conditions controlling the crystallization process of the orbicules. Geochemical differences between Pl and Hbl pairs in the zones identified in the orbicule could respond to significant variations in the crystallization conditions, as is suggested by the different textural characteristics. However, the results obtained for the shell should be taken with caution because the radial arrangement and feathery textures can be produced by supersaturation or undercooling processes, indicating significant departures from the Hbl-Pl equilibrium needed to achieve reliable data on thermobarometry.

Table 2 shows the temperature values obtained using Hbl–Pl equilibrium after multiple iterations as a function of pressure. Geochemical compositions of Hbl and Pl used for these calculations are presented in Annex 2. All thermometry results are referred to HB2 temperatures calibrated according to the reaction edenite + albite = richterite + anorthite (Holland and Blundy, 1994). As a first approach, we used 2 and 4 kbar as arbitrary pressures, which is the pressure range assumed for the emplacement of Jurassic plutons in the region (e.g. Rodríguez et al., 2016). We also have used the calculated pressures according to calibrations of the Al-in-hornblende barometer (Anderson and Smith, 1995; Schmidt, 1992), which yield results mostly within the range indicated above. A comparison of the geochemistry of the Pl, Hbl and Cpx crystals analyzed in the different zones of the orbicular body are presented in Fig. 5, together with the thermobarometry results.

Results in the orbicular core are obtained from Pl labradotite external rims and unzoned Hbl, resulting in temperatures between 880 and 835 °C (Table 2, Figs. 4b, 5). Lower temperatures are obtained from small Pl crystals included in Hbl. In the orbicular shell, hornblende–plagioclase pairs are analyzed at both Ca-rich and

Table 2
Results of Hbl-Pl thermobarometry.

Sample	Hbl	Pl	2 Kbar	4 Kbar	Schmidt		A&S
			T (°C)	T (°C)	T (°C)	P (Kbar)	T (°C)
GO-N (core)	GO-5	GO-7	883,9	889,4	888,5	3,67	876,7
	GO-8	GO-10	843,2	849,5	847,5	3,38	838
	GO-16	GO-18	841	847	845,6	3,53	836,6
GO-O (inner shell)	GO-24	GO-26	955,5	963,6	961,6	3,50	935,3
	GO-24	GO-25	841,3	848,7	846,9	3,50	835,8
	GO-28	GO-33	941,4	948,8	947	3,50	924,7
	GO-28	GO-34	838,6	845,3	843,6	3,50	833,7
	GO-40	GO-37	903,1	910,8	907,5	3,13	889,8
	GO-40	GO-38	810,1	817,2	814,1	3,13	806,5
GO-O (contact)	GO-61	GO-59	869,9	876,8	879,1	4,70	864,9
GO-M (matrix)	GO-72	GO-74	910,8	915,4	915,0	3,80	902,8
	GO-85	GO-74	881,5	887,3	887,6	4,11	874,9

T (°C): HB2 temperature in Holland and Blundy (1994).
2 and 4 Kbar: results based on an arbitrary pressure.
Schmidt: pressure-based results according to Schmidt's (1992).
A&S: pressure-based results according to Anderson and Smith's (1995).

Ca-poor patches of Pl that are indistinctly in contact with large elongated unzoned Hbl crystals (Fig. 4c, d and e). While Ca-rich plagioclases (85 mol% An) yield the highest temperatures, between 935 °C and 890 °C for the inner shell (according to AandS temperatures, Fig. 5, Table 2), Ca-poor patches (70 mol% An) show lower temperatures, which vary from 835 to 806 °C. The results obtained in the outer shell and in the matrix, which are analyzed in Pl crystals with concentric zoning, vary between 900 and 865 °C (Fig. 5, Table 2).

Pressure estimations according to the technique of Schmidt (1992) are of around 3.5 kbar from the core to the outer shell of the orbicule (Fig. 5, Table 2), with a significant increase in the orbicule contact and the matrix (4.7 to 4 kbar respectively).

Thermobarometric results evidence the differences between the crystallization processes in the orbicular core, inner shell, outer shell and matrix. Although the heterogeneous crystallization in the orbicular shell does not allow to define the temperature or pressure conditions during the radial crystallization, the thermobarometric and geochemical results show notable differences that are in agreement with the textural descriptions. Moreover, the equilibrium temperatures and pressures obtanied in the orbicular core and matrix establish the thermobarometric limits during the orbicular magma crystallization.

4.4. Study of the crystallographic preferred orientation (CPO) of quartz

The analyzed crystals are large interstitial quartz grains from the inner shell (area 5, Fig. 6), the outer shell (areas 2, 3, 4, Fig. 6), and the matrix (area 1, Fig. 6). The studied areas include only one or two crystals, with occasional undulatory extinction or subgrain domains. Therefore, EBSD patterns are typical of mono-crystal orientations, with prominent [*c*] axis maxima and three well-defined concentrations of ⟨*a*⟩ axes. Undulatory extinction produces slight scattering around the main maxima. Orientation of the [*c*] axis of quartz crystals in the inner shell is normal to the core-shell boundary, and parallel to the long axes of the large Pl and Hbl elongate crystals. In contrast, quartz [*c*] axes in the outer shell and contact zone are parallel to the orbicule boundary and to the concentric crystals of Pl and Hbl. Oblique orientations have been determined for quartz [*c*] axes in the matrix zone relative to the external contact of the orbicule. In summary, it can be stated that the crystallographic orientation of the interstitial quartz crystals mimics that of the Pl + Hbl framework in the orbicule and its matrix, reinforcing the idea that the process generating the orbicular texture was active during the entire period of crystallization of the involved magmas and fluids.

5. Whole rock geochemistry

5.1. Analytical techniques

Major and trace elements were analyzed by X-ray fluorescence (XRF) and inductively coupled plasma mass spectrometry (ICP-MS) respectively, at the Actlabs Laboratories (Coquimbo, Chile). Major elements were analyzed using the PHILIPS PW 2400 Wavelength Dispersive X-ray Fluorescence Spectrometer. The total uncertainty is determined to be ±100% at the detection limit, ±20% at 10 times the detection limit and ±5% at 100 times the detection limit (relative percentages). Trace elements, including rare earth elements (REE), were analyzed with an Perkin Elmer Sciex ELAN 9000 ICP-MS. Samples are fused with Na_2O_2 at 650–700 °C for 30 min in a Zirconium crucible. The fusion cake formed in the crucible during this process is dissolved in purified water and acidified (room temperature digestion) with concentrated nitric and hydrochloric acids. The total uncertainty is determined to be ≤100% at the detection limit, ≤30% at 10 times the detection limit and ≤20% at 100 times the detection limit (relative percentages).

5.2. Geochemistry results

Core, shell, and matrix, the three textural and compositional parts composing the orbicular granitoid of Caldera, were analyzed with the aim of studying the compositional relations between the different orbicular parts and to discuss the processes suggested for the formation of the radial orbicular textures (Table 3, Figs. 7, 8 and 9). Besides, the host-rock granitoid sampled 100 m to the NE of the orbicular body was also analyzed. For comparison purposes, the geochemical data of Aguirre et al. (1976) have also been considered (Figs. 7, 8). Note that the matrix and shell data from the work of Aguirre et al. (1976) are calculated based on modal analysis. Also, we have estimated a mean composition for the orbicular granitoid (WR) corresponding to a weighted average. By image analysis, we calculated the proportion of the different components forming the orbicular granitoid (core, shell and matrix). The image analysis was carried out using 10 images, taken as representative of the whole orbicular body. The resulting proportions (0.13 for the orbicule core, 0.4 for the shell and 0.47 for the matrix) were used to determine the mean composition (WR) of the orbicular granitoid (Table 4).

According to the TAS classification diagram (Le Bas et al., 1986) (Fig. 7a), the orbicular shell (including inner and outer parts) plots in the field of gabbro, the matrix falls on the compositional field of granodiorites and the core and host-rocks have a dioritic or tonalitic composition. Together, the orbicular samples are calc-alkaline, metaluminous and magnesian rocks (Fig. 7a, b and c). Harker variation diagrams (Fig. 7d–j) show similar compositions for orbicular cores, non-orbicular inclusions (Fig. 2f) (Aguirre et al., 1976) and tonalitic host-rocks, with lower TiO_2 and higher Al_2O_3 and CaO contents in the core, which presents the most basic composition of this group (Table 3, Fig. 7d, e and f). The weighted average composition of the orbicular body is similar to the host tonalite. These samples are projected in an intermediate location between the gabbroic Mg, Fe and Ca-rich shell and the K-rich granodioritic matrix in all the variation diagrams. Shell and core XRF analyses are similar to those of Aguirre et al. (1976), but matrix XRF data show higher silica contents.

The CaO vs MgO and molar $K_2O/(K_2O + CaO)$ vs MgO diagrams (Fig. 8a, b) show similar relations to that observed in Harker diagrams between the studied samples. The orbicular core and the host-rock sample are plotted between the Ca—Mg rich shell and the Mg-poor, K-rich matrix. In terms of magmatic fractionation, the evolution of liquid compositions by substraction of Pl + Hbl or Pl + Cpx describes hypothetical trends between the different orbicular compositions. In this sense, the evolution of liquid compositions derived from a dioritic parental magma (black lines, Fig. 8a, b) with 2 wt% of H_2O and 4 kbar

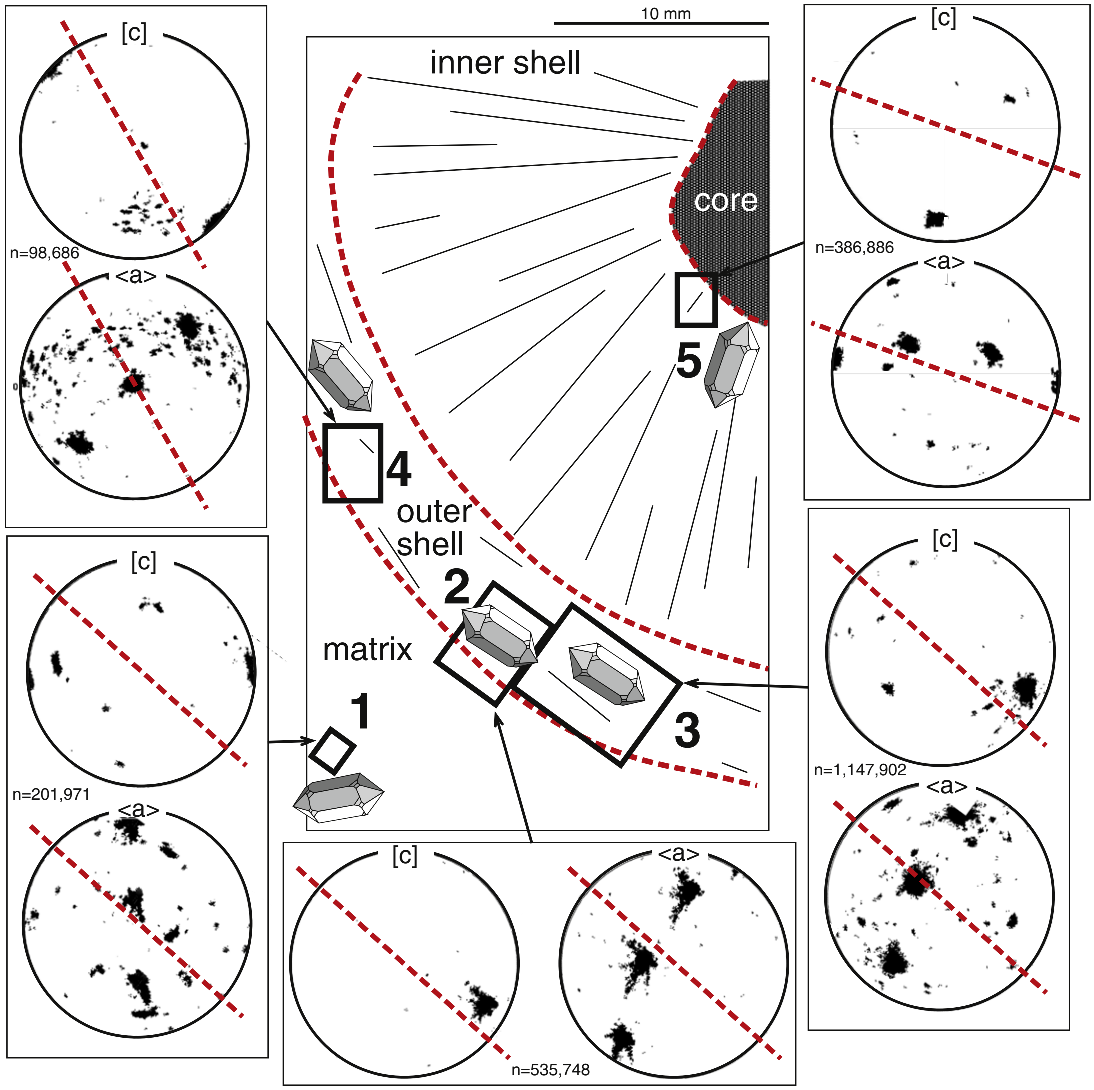

Fig. 6. Sketch of the sample measured with EBSD-SEM. The distinct zones of the orbicule (core, inner and outer shell) and matrix are schematically represented, together with the radial (inner shell) and concentric (outer shell) fabric of the Pl-Hbl framework. Crystallographic preferred orientation of quartz crystals of selected areas (1 to 5) are shown with pole figures (equal-angle, lower-hemisphere projection of [*c*] and ⟨*a*⟩ axes; n: measurement points). Dashed red lines in the sketch and pole figures represent the orientation of the contacts between the zones of the orbicule. Bipyramidal forms schematically depict the average orientation of the quartz crystals in the distinct zones of the orbicule, according to the results shown in the stereoplots.

as initial conditions, calculated with Rhyolite-MELTS (Ghiorso and Sack, 1995; Gualda et al., 2012), approximately matches the compositions of the orbicular components. However, this geochemical link must be taken carefully because the textural characteristics of the studied orbicular rocks are clearly pointing to a process of desequilibrium crystallization.

Highly compatible elements (Sc, Ni, Co or Cr) are enriched in the orbicular shell and depleted in the matrix. On the contrary, large-ion lithophile elements, such as Rb or Ba, are significantly enriched in the granodioritic matrix (Table 3). As an example, Cr and Rb (Fig. 8c) show inverse contents in the shell (Cr-rich gabbro) and the matrix (Rb-rich granodiorite). These differences are related to the different mineral concentrations, i.e. shell composition is richer in Cr due to the higher magnetite content and poorer in Rb because of the lower K-feldspar fraction. The orbicular core and the host-tonalite show, as described for major elements, trace element contents intermediate between those of the matrix and the shell.

Strong fractionation of highly compatible and large-ion incompatible elements is not correlated with rare earth elements (REE) patterns (Fig. 9a), which show only slight differences between the orbicular core, shell, matrix and host-rock. The four samples present almost parallel patterns with Ce^N/Yb^N ratios within the range 3.36–3.91. Main differences appear in the HREE between the orbicular shell and the matrix, with Yb^N values of 19.26 and 14.9, respectively. Sr/Y ratios are positively correlated with the slight differences found in the #Mg (Fig. 9a). However, it is remarkable that the gabbroic shell and the pegmatitic granodiorite matrix have similar values in $Eu/Eu^* = 0.66$ and 0.56 and $\Sigma REE = 109.2$ and 93.48, respectively.

The unequal behavior between strongly compatible (Sc, V, Cr, Co) and incompatible (Rb, Ba) elements, on one side, and the REE, Sr, and Y, on the other side, is clearly illustrated by taking a simple ratio between the distinct elementary contents analyzed in the orbicular shell and matrix (Fig. 9b). Fig. 9c and d show the theoretical distribution of trace elements calculated for fractional crystallization according to the equation (e.g. Rollinson, 1993),

$$C_R/C_0 = D * F^{(D-1)}, \text{ where } C_R \text{ is the instantaneous solid, } \quad (1)$$
$$C_0 \text{ is the parental liquid, D is the bulk partition coefficient}$$
$$\text{and F is the fraction of remaining liquid}$$

Table 3
Whole rock geochemistry results.

Rock type	Orbicular core	Orbicular shell	Orbicular matrix	Host granitoid
Sample	GO—N	GO—O	GO—M	GO—E
Wt%				
SiO_2	56,1	48,95	68,13	59,65
TiO_2	0,33	0,56	0,51	0,83
Al_2O_3	18,97	17,86	14,72	16,28
FeO	5,62	9,58	4,07	6,66
MgO	3,14	5,63	1,9	3,47
MnO	0,08	0,16	0,04	0,11
CaO	9,35	11,75	5,37	6,37
Na_2O	2,97	2,33	2,21	3,03
K_2O	1,11	1,16	2,34	1,73
P_2O_5	0,15	0,14	0,08	0,13
LOI	0,97	0,82	0,72	0,69
Total	98,78	98,94	100,1	98,95
ppm				
Li	8	15	17	22
Sc	20	45	18	23
Be	1	1	1	1
V	208	523	177	191
Cr	50	90	30	60
Co	17	28	13	19
Ni	20	40	*d.l.*	*d.l.*
Cu	40	90	370	40
Zn	50	100	60	70
Ga	21	22	15	17
Rb	32	45	75	71
Sr	276	270	236	205
Y	30	28	30	26
Zr	78	52	222	166
Nb	1	2	2	5
Cs	2,7	3,5	3,2	4,8
Ba	116	118	479	264
La	18,5	17,3	14,2	18,6
Ce	43,2	39,6	32,1	41,1
Pr	5,79	5	4,32	5,02
Nd	23,9	20,3	18,8	20,5
Sm	6,1	5,2	5	4,8
Eu	1,39	1,16	0,93	1,12
Gd	6	5,6	5,1	4,9
Tb	1	0,9	0,9	0,9
Dy	5,9	5,8	5,2	5
Ho	1,2	1,1	1	1
Er	3,3	3,2	2,8	3
Tm	0,45	0,48	0,4	0,45
Yb	2,9	3,1	2,4	3
Lu	0,42	0,49	0,33	0,46
Hf	2,1	1,3	4,7	4,1
Ta	0,2	0,2	0,2	0,5
Pb	7	7	132	10
Th	8,7	4,2	6,4	7,2
U	1,7	1	1,3	1,5

d.l.: detection limit.

The solid assemblage is conformed by Cpx (5%) + Pl (52%) + Hbl (42%) + Mag (1%), a modal estimation of the assemblages observed in the shell (Figs. 3 and 4). We have used partition coefficients (K_D) for andesitic liquid compositions (Supplementary material, Annex 3), which must correspond to the parental magmas in a continental active margin context (Kelemen et al., 2003). A range of K_D values has been used in order to model different trace element behaviors, and the lowest and highest K_D have been plotted separately in Fig. 9c and d respectively (see values and references in Annex 3). The results show the strong fractionation of Cr, Co, V and Sc (enriched in the instantaneous solid), and Rb and Ba (enriched in the residual liquid), besides the slighter enrichment of REE in the residual liquid. However, high K_D values promote the compatible behavior of elements as Sm, Sr, or Eu (Fig. 9d). The relation between the theoretical behavior expected for trace elements in a process of fractional crystallization and the REE patterns found in the orbicular samples is an essential feature to evaluate the possible processes that generate these textures and will be discussed later.

The analyzed orbicular samples show the typical relative depletion in Nb and Ti and enrichment in Ba, Rb, Th, and K, characteristic of arc settings (Fig. 9e). Again, these elements, as well as Hf and Zr, present a strong fractionation between the orbicular shell and the matrix. In contrast, REE present very similar contents in shell and matrix (Fig. 9e, Table 3).

6. Crystallization models

In order to gain insight into the magma evolution and the crystallization process giving rise to the orbicular granitoid, we performed thermodynamic modeling with the MELTS-Rhyolite code (Gualda et al., 2012). The pressure of emplacement ranges from 4 to 3 kbar according to the thermobarometry calculations. The redox conditions are set at QFM + 2 buffer as representative for the cordilleran batholiths (Brandon and Draper, 1996; Carmichael, 1991; Parkinson and Arculus, 1999) and to satisfy the requirements of the crystallization sequence.

We selected different compositions for the starting material with the aim of covering a wide range of starting conditions. The mean composition (WR) of the orbicular granitoid (Table 4), the orbicular core (GO-N) and the host granitoid composition (GO-E) were used for the thermodynamic modeling. As the composition of the host rock (GO-E) and that estimated for the whole orbicular granite (WR) are very similar (Fig. 7), the modeling results overlap. For this reason, we only show the orbicular granite (WR) and the orbicular core composition tests in Fig. 10. The composition of liquids and residues for each model, at crystallization intervals of 10%, and the corresponding mineral modes are listed in Tables S1 and S2 (Supplementary material, Annex 4), respectively. The initial polymerization degree of the distinct melts involved in the process has been estimated through the calculation of the NBO/T parameter. Results (0.35, 0.12 and 0.07 for shell, core and matrix, respectively) agree with the expected values determined in similar silicic melts (e.g., Iezzi et al., 2009).

Amphibole stabilization has not been reached for any model. Nonetheless, amphibole addition has been considered for the modeling discussion, because amphibole is a major phase in these rocks. The addition of an increasing fraction of amphibole to the residue compositions, instead of the Cpx fractionation, would produce a CaO enrichment of the liquid compositions because of their lower CaO content (Fig. 10a and b). At the same time, the Amp precipitation instead of Cpx involves that the K/K + Ca ratio would be decreased due to the increase of CaO content in the liquid compositions (white arrow in Fig. 10c and d). Pressure effect on the liquid and residue compositions, ranging between 3 and 4 kbar, is almost negligible (Fig. 10).

For those cases with WR as starting material and low water contents, residue compositions match the shell composition (GO—O; Fig. 10a and b). However, if we add the Amp input to the residue composition, models with the orbicule core (GO—N) as starting material can also reproduce the shell composition. The K/K + Ca ratio (Fig. 10c and d) gives information about the shell behavior as a cumulate. The modeled residue compositions do not match the K/K + Ca ratios of the orbicular shell. The explanation is that residues modeled by MELTS code do not preserve the residual liquid corresponding to the terminal porosity (Lee and Morton, 2015) that finally solidifies as K-feldspar and quartz enhancing the K/K + Ca ratio of the orbicular shell.

Liquid lines for all cases evolve towards more differentiated compositions approaching, in the cases in which the initial water content is low, the matrix composition (GO—M) when the crystallinity is between 40 and 50% (Fig. 10). However, if we consider Amp fractionation instead of Cpx, the liquid lines would move away from the matrix composition. Considering the composition of the matrix (GO—M), we can observe that the Ca content (5.37 wt%; Table 3) is greater than the expected value for this evolved composition with 68.13 wt% of SiO_2 (Table 3).

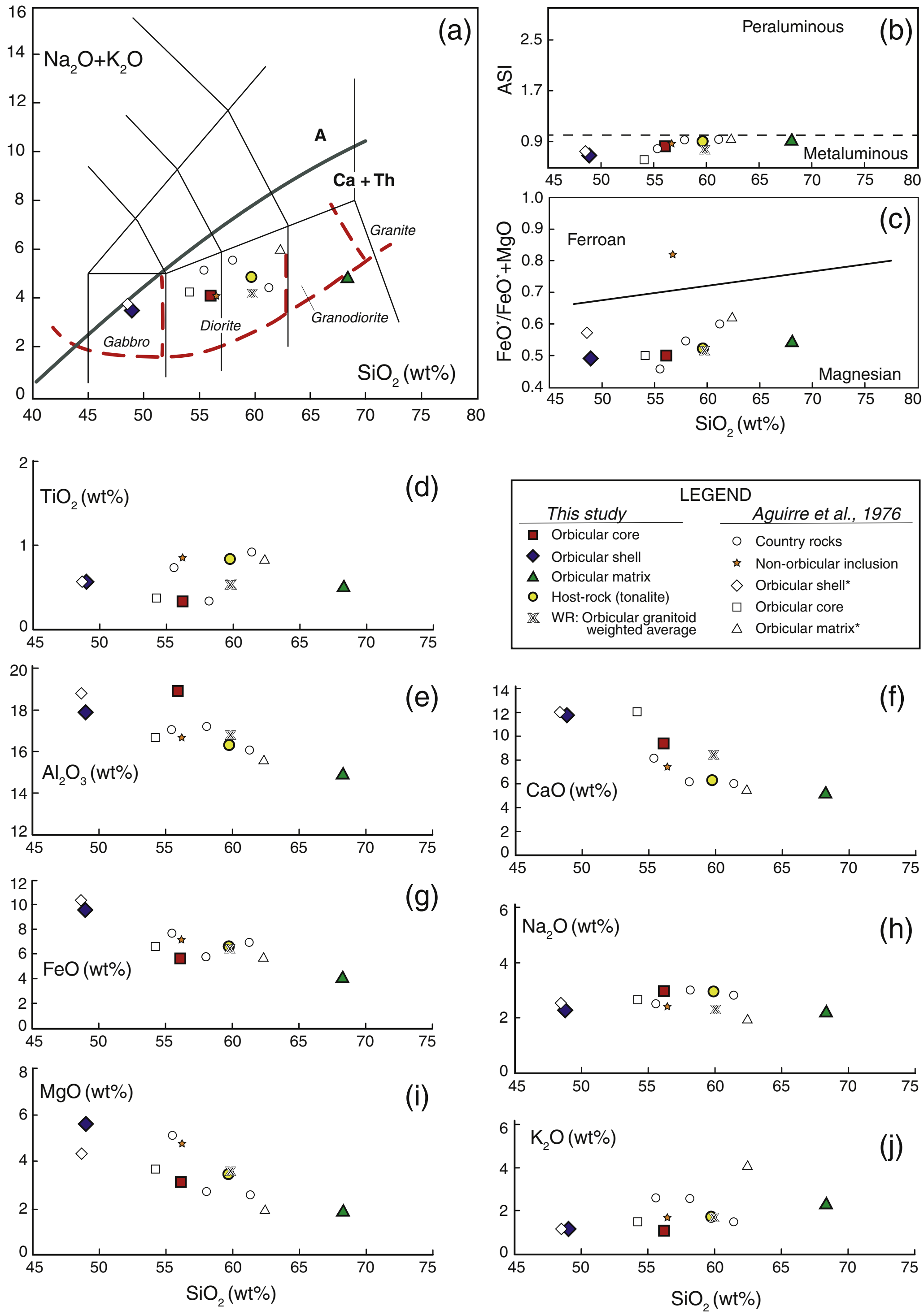

Fig. 7. General compositional features of the orbicular core, shell and matrix and the host rocks of the orbicular body. (a) TAS (Total alkalis vs silica) classification diagram (Le Bas et al., 1986). The fields divided by the dashed lines are based on the TAS diagram adaptation for plutonic rocks (Wilson, 1989). The curved solid line separates the alkaline and calc-alkaline/tholeiitic series. (b) (c) Aluminum Saturation Index (ASI) and #Fe vs. silica granitoid classification diagrams (Frost et al., 2001). (d–j) Silica variation (Harker) diagrams. Geochemical results obtained by Aguirre et al. (1976) are presented for comparison.

This fact can be the result of previous massive amphibole precipitation, giving rise to a differentiated residual liquid with a large Ca content. The high water activity in the entire system during the volatile exsolution and the water-rich residual liquid triggered by shell crystallization can explain this massive stabilization of a hydrous phase and the composition of this residual liquid (GO—M).

7. Discussion

This paper describes the textures present in the orbicular granitoid of Caldera (Chile) and its geochemical characteristics, main tools to discuss the processes that drive the intrusive magma to yield the orbicular structures. The analysis of the textures, the geochemical results and the

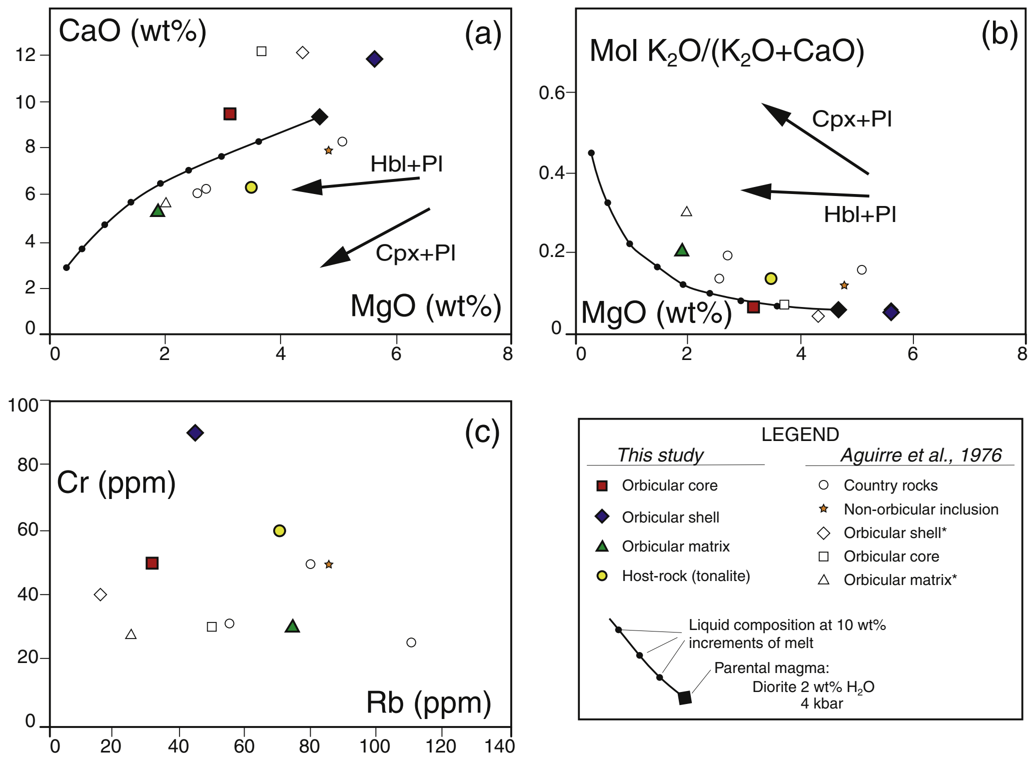

Fig. 8. Major and trace element geochemical diagrams showing relevant compositional variations among the different parts that comprise the orbicular body and the host granitoid. (a) (b) CaO and Mol $K_2O/(K_2O + CaO)$ vs. MgO. Black lines and dots represent model liquid compositions calculated with Rhyolite-MELTS (Ghiorso and Sack, 1995; Gualda et al., 2012) for a dioritic parental composition. Arrows represent theoretical fractionation vectors that agree fairly well with the direction of the ideal fractionation between the gabbroic shell and the granodioritic matrix. (c) Cr vs. Rb variation diagram shows a "normal" compositional variation between trace elements for gabbroic and granodioritic compositions.

petrogenetic modeling, are the basis to argue for a complex crystallization process that must take into account the crucial role of water and the possible segregation of two liquids or silicate gels with different viscosities.

7.1. Where do orbicular granitoids occur?

Radial and concentric orbicular structures have been described for a wide variety of plutonic compositions, among others: gabbros, Kfs-rich magmas and granitoids enclosing Crd-rich host rock xenoliths (Abdallah et al., 2007; Aguirre et al., 1976; Grosse et al., 2010). However, the bibliography devoted to the study of these orbicular textures highlight the fact that the orbicular bodies are mostly located at the margins of intrusive complexes, where mafic rock domains and magma-host rock interactions are more abundant. In the examples where the orbicular cores, also called "cold germs" (Decrite et al., 2002), are interpreted as fragments of granitic rock, these must have been dragged from the host rock or crystal mush where the orbicular magma is emplaced.

The orbicules of Caldera present a texturally and compositionally distinguishable core, which shows similar geochemical characteristics to the host tonalites of the Relincho pluton (Fig. 7), sampled 100 m to the NE of the orbicular body. However, these cores present a slightly more basic composition than the host tonalites, with lower SiO_2, and higher Al_2O_3 and CaO contents, but almost identical FeO and MgO. This coincides with a greater abundance of Pl (bytownite) in the orbicular core relative to the host granitoid far from the contact. Furthermore, the lobulated and magmatic contacts between the orbicular body and the host rocks (Fig. 2) show no evidence of solid state or brittle deformation, pointing to a magmatic interaction between both granitoids.

We propose here a crystallization front setting for the emplacement of the orbicular magma. There is not any field or geophysical evidence attesting to the nearby presence of the external, western contact of the Relincho pluton. Nevertheless, the geochemistry and mineralogy of the orbicular cores is compatible with that of a Pl-rich crystal mush (Marsh, 1996) from the host granitoid magma. The same has been proposed for other orbicular bodies (e.g. Grosse et al., 2010). The irregular shape of these cores (Fig. 3) also points to solid crystal assemblage fragments detached from the crystallization front of the host Relincho pluton. A reliable water source, which plays a crucial role during the crystallization of radial textures, can be found in the water-rich residual melt expected in this high crystal fraction mush. Therefore, the contact between the orbicular and the host magmas operated as an open system, providing crystal mush fragments and a H_2O-rich liquid to the intruding magma, probably until the crystallization of the Pl-Hbl radial assemblage observed in the contact.

Orbicules, as most magmatic structures, are the result of the interaction between crystals, volatiles and melt during successive magma inputs (Vigneresse, 2014). Regarding the analysis of the physical conditions of the host magma and the inception of the structure and space needed for the new magma batch to emplace, a complex interplay between viscous flow and brittle behavior in granitic magmas has been described (Fernández and Castro, 1999; Rubin, 1993). Middle crust conditions at a convergent plate boundary setting are suitable to trigger transient brittle behavior of a partially crystallized magma (Fernández and Castro, 1999), allowing the interaction between the host and the intrusive magma according to the characteristics observed in the orbicular granitoid of Caldera.

7.2. Why do radial orbicular textures occur?

There is significant agreement on the fundamental role of water in the formation of radial orbicular textures (e.g. Vernon, 1985; Waters et al., 2015). Experimental petrology assesses the generation of these textures studying the temperature gradients and experimental temperature vs. time cooling ramps needed to relate undercooling rates with

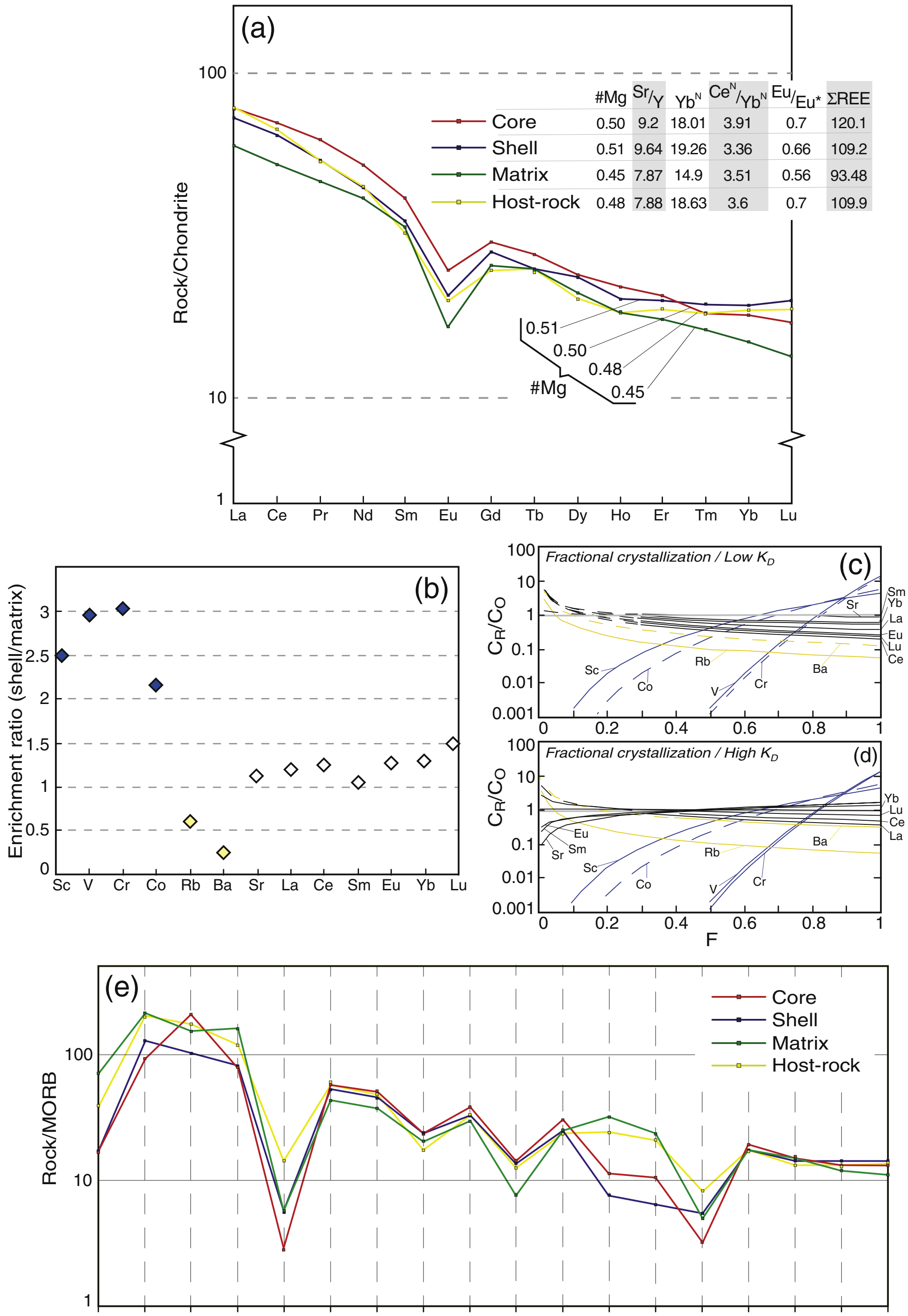

Fig. 9. (a) Chondrite-normalized (Nakamura, 1974) REE diagrams for the orbicular body components and host granitoid. Inset shows the main trace element ratios. REE patterns show no correlation with any fractionation factor (e. g. Mg-number). (b) Enrichment ratio (shell/matrix trace element concentrations) for main compatible and incompatible trace elements and REE. (c) (d) Theoretical trace element distributions for low and high K_D fractional crystallization, showing the differences with the concentrations analyzed in the orbicular shell and matrix. See text for further details. (e) Thompson normalization plot rock/MORB for the orbicular body components and host granitoid.

columnar crystallization and to explain the origin of tabular, skeletal, dendritic, spherulitic or feathery textures (e.g. Lofgren, 1974). However, these sharp temperature or pressure changes are not usually described in plutonic settings. The alternative possibility of superheating and undercooling processes can be studied through the use of T—P—H_2O phase diagrams to calculate the needed H_2O (e.g. Naney, 1983). In fact, most of the studies on orbicular structures agree that effective superheating could be caused by injection of water into an intermediate magma (e.g. Vernon, 1985), which reduces the liquidus temperature of the magma promoting melt depolymerization (e.g. Fenn, 1977; London, 1992). Besides, this superheated liquid may contain minerals or rock fragments from the host mush or rock that can act as nucleation seeds. The geochemical, textural, and morphological characteristics of the orbicular granitoid of Caldera suggest that three main processes should operate simultaneously during the formation of radial orbicular structures: 1) crystallization of a gabbroic solid assemblage that

Table 4
Whole rock composition modeled by image analysis.

wt (%)	GO
SiO_2	59.64
TiO_2	0.51
Al_2O_3	16.76
FeO	6.58
MgO	3.61
MnO	0.10
CaO	8.57
Na_2O	2.39
K_2O	1.73
P_2O_5	0.11
Total	100.0
K/K + Ca*	0.11

* K/(K + Ca) = molar ratio $K_2O/[K_2O + CaO]$.

segregates a granodioritic residual liquid, as is concluded by the geochemical characteristics of the different components of the orbicular body and the Rhyolite-MELTS models, 2) heterogeneous columnar and radial crystallization under undercooling conditions indicated by the feathery textures in the orbicular shells and 3) immiscibility or segregation of two liquids or silicate gels according to the shape of the orbicules and the textures described in the orbicule-matrix contact.

Indeed, major and some trace elements evidence a fractionation process between the orbicular shell and the matrix, while the parental orbicular magma would present a composition similar to the host granitoid, i.e. the orbicular core. The cotectic Pl + Cpx fraccionation trends link the major element compositions of the solid assemblage (the shell, where the Pl and Cpx crystals of the observed paragenesis are interpreted as liquidus phases, Fig. 3) and the residual melt (the matrix, Fig. 8), as is endorsed by crystallization models. From the modeling results, we can deduce that the crystallization from a parental magma with a composition close to the orbicule core is plausible. When the crystallinity reaches a fraction between 0.4 and 0.5, modeled solids and residual liquids match those compositions obtained for the orbicular shell and matrix. Then, the crystallization conditions change to the stability field of amphibole (Fig. 10) by the Cpx ➔ Hbl reaction in presence of a SiO_2 and H_2O-rich residual liquid (Cpx pseudomorphs and cores in radial Hbl, Figs. 3 and 5) (e.g. Castro, 2013). The modal volumetric estimations of the shell and the matrix in the orbicular body match those fractions of the solid assemblage and the residual melt obtained by the modeling results. Main compatible (Cr, Sc, V, Co) and incompatible (Rb, Ba) trace elements are also fractionated according to the distribution coeficients (K_D) calculated for the paragenesis observed in the orbicular shell (Fig. 9b, c and e). However, the REE, Sr, and Y contents do not evidence this fractionation process, (Fig. 9a and e). Partition coefficients close to the unity for some trace elements in undercooling or low temperature (migmatization) processes are described as a consequence of the crystal-liquid disequilibrium (Bea et al., 1994; Henderson, 1986). Therefore, the dissimilar behavior of trace elements does not exclude the fractionation process, but it is rather pointing to a process of heterogeneous crystallization related to undercooling conditions.

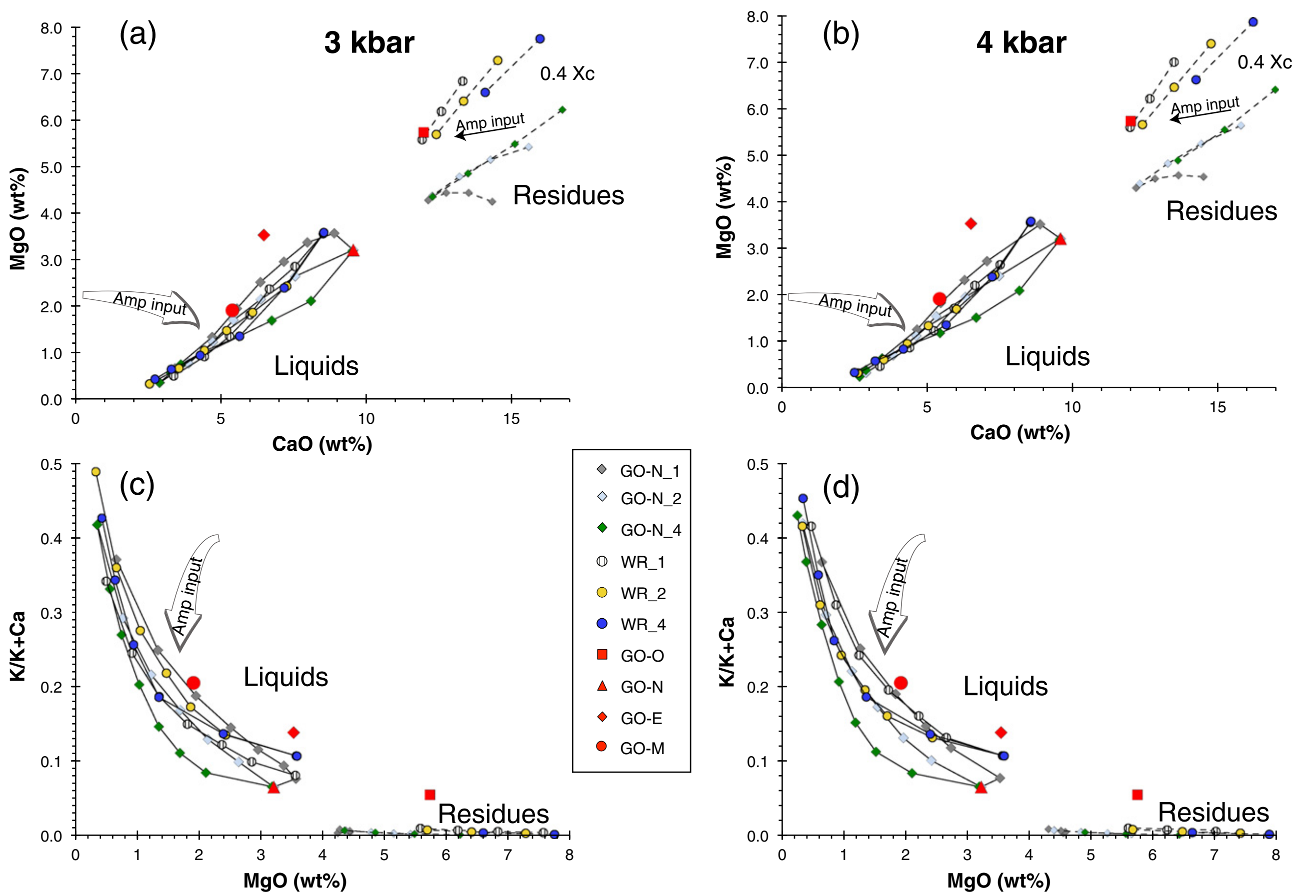

Fig. 10. Geochemical variations diagrams from thermodynamic modeling results carried out using the MELTS-Rhyolite code (Gualda et al., 2012). Starting materials are referred as GO-N (orbicule core), WR (estimated composition for the orbicular granitoid). The initial water content, varying from 1 to 4 wt%, is specified by the number following the reference (i.e. modeling results for the orbicule core as starting material and 1 wt% of initial water content are represented by GO-N_1). The analyzed compositions of the orbicule (GO—O), core (GO—N), host rock (GO—E) and matrix (GO—M) are also represented for comparison. Liquids are represented at crystallization intervals of 10%, by solid lines. Residues are represented by dashed lines, only from 40% crystallinity until calculations converge. (a) (b) CaO vs MgO diagrams showing the evolution of liquids from the *liquidus* to the end of crystallization for pressures of 3 and 4 kbar, respectively. (c) (d) MgO vs K/K + Ca ratio diagrams for pressures of 3 and 4 kbar, respectively.

The globular or spherical shape of the orbicules (Fig. 2) and the contact relations between the orbicular shell and matrix (Figs. 3, 6) indicate the presence of two liquids, melts or gels with distinct viscosities and concurrent crystallization processes close to the contact in both sides of the orbicule boundary. The rounded orbicular shapes recall the contact relations of typical mafic enclaves in calc-alkaline batholiths (e.g. Castro et al., 2008), which are generated during the mingling of two magmas with different viscosities. Ballhaus et al. (2015) propose the exsolution of an immiscible solute-bearing H_2O-dominated fluid phase at elevated temperature and pressure promoted during H_2O saturation. The presence of a H_2O-rich superheated liquid, that evolves expelling the volatile excess, triggers the undercooling conditions promoting the heterogeneous columnar crystallization. Around the host-rock fragments or cold germs, during the volatile exsolution, the mafic H_2O-rich silicate melt underwent a sudden crystallization that gave place to the radiate textures (Figs. 3, 6). Spherulitic Hbl crystals in the inner shell do not show significant compositional differences, which is consistent with isothermal conditions during the rapid crystallization of the orbicular shell (Fig. 5). However, reverse zoning in plumose Pl and Px crystals has been related to disequilibrium crystallization during rapid undercooling, also under isothermal conditions (Durant and Fowler, 2002; Grosse et al., 2010).

The contact between orbicular shell and matrix is characterized by the Hbl and Bt oikocrystals that grow over radial Pl crystals in the outer shell, and include small rounded crystals of Pl and Mag in the matrix contact (Fig. 3). Geochemically, Hbl oikocrysts show lower #Mg than the radial Hbl of the inner shell (Fig. 5). Both the small grain size of the Pl crystals in the matrix contact and the poikiloblastic textures are indicative of a rapid crystallization process close to the solidus, and are similar to the textural domains described in pegmatites (London, 2009). The constant disposition of the oikocrysts around the orbicule, which are systematically orthogonal to the radial Hbl of the inner shell, suggests that the crystallization of the outer shell and the matrix were simultaneous. The pegmatitic domains of the orbicular matrix, located in the inter-orbicule spaces, represent the H_2O-rich residual liquids exsolved from the shell (Jahns and Burnham, 1969).

The processes of geochemical fractionation relating the orbicular shell and matrix, coalescence of two liquids or gels, and undercooling-promoted columnar crystallization, evolved in the context of a superheated intrusive magma, must be rapid and almost simultaneous. Similar crystallization sequences have been obtained experimentally. Initial feathery or "bow tie" textures followed by radial spherulitic crystallization are formed in the course of a few hours (Arzilli et al., 2015). Highest estimated growth rates are around ~10 μm^3 in 1 s (Arzilli et al., 2015; Spillar and Dolejs, 2013), or on the order of 1 to 5 mm per day (Fenn, 1972; Lofgren, 1974).

7.3. Building a model for generation of the orbicular granite of Caldera

Most studies about orbicular structures agree that effective superheating could be caused by injection of water into the orbicular magma (e.g., Vernon, 1985). Let us suppose that a new magma batch is emplaced within the crystallization front (Marsh, 1996) of a magma body through a magmatic fracture caused by the brittle behavior of the viscous host magma (Fernández and Castro, 1999). In that case, H_2O-rich residual liquids would be able to migrate towards the new magma batch from the partially crystallized host magma (Relincho pluton), while crystalline fragments can be dragged from the crystal mush and incorporated into the new magma batch, constituting the cores of the future orbicules (Fig. 11). The relative motion between the two magmatic bodies and their viscous behavior generated the lobulated contact relations observed in the orbicular granitoid (Fig. 2). The residual liquid from a host magma with a high crystal/liquid ratio is too close in composition to silica-rich leucogranites (Johannes and Holtz, 1996; Winkler and Lindemann, 1972). What would be, instead, the putative composition of the new magma batch? A dioritic magma composition is more favorable to generate the gabbroic assemblage of the orbicular shell, according to the geochemistry and crystallization modeling results (Figs. 7 and 10).

The H_2O released by the host crystal mush was carried to the low pressure area generated in the magmatic fracture, where these volatiles were dissolved in the new dioritic magma. According to thermobarometric data, this process occurred below 850 °C and at around 3.5 kbar (Fig. 5). The geochemical composition of the new magma batch is similar that of the host granitoids. Consequently, they may share the same source area and P–T conditions, where they were previously fractionated as suggested by the Eu anomalies observed in the studied orbicules (Fig. 9a and e). The high influx of H_2O-rich liquids induced superheating conditions in the newly intruded magma that became a depolymerized liquid, where the only remaining solid particules, seeds or cold germs were the small irregular fragments of the host granitoid magma dragged from the fracture walls (Fig. 11).

Afterwards, the H_2O-rich superheated magma exsolved the volatile excess to reach the equilibrium at the emplacement conditions (or the minimum water necessary to maintain the *liquidus* temperature). The volatile loss promoted the sudden or "explosive" crystallization under undercooling conditions. Undercooling temperature changes of around 80–100 °C, like those estimated experimentally for basaltic compositions (Lofgren, 1974), are equivalent to 3–4 vol% of H_2O loss according to experimental phase diagrams of Naney (1983). Crystallization of the solid paragenesis occurred on the host rock fragments. Crystallization of feather-like large crystals took place at embayed contacts, while in more planar limits, acicular crystals grew orthogonal to the contact. This rapid crystallization is isothermic and did not induce geochemical variations in the Pl + Hbl assemblage of the inner shell. Undercooling and nucleation around the core (cold germs) promoted the physical and geochemical fractionation between two sub-systems: 1) a gabbroic sub-system (Figs. 7, 8 and 9) that comprises the solid paragenesis Pl + Cpx + Hbl + Mag and a residual H_2O-rich liquid and 2) a granodioritic sub-system. The heterogeneous crystallization fractionated major and some trace elements (e.g. Cr, Sc, Ba, Rb) (Fig. 9) between the sub-systems, while REE, Sr or Y show distribution coefficients close to the unity and were not fractionated. The presence of a H_2O-rich residual liquid in contact with the solid paragenesis in the gabbroic sub-system triggered the almost complete resorption of Cpx and its substitution by Hbl in the inner shell (Fig. 11) when the crystal fraction reached around 0.4–0.5. The orbicules, including core and shell, behaved as viscous bodies (crystals + residual liquid) floating in the granodioritic magma. According to the shape preferred orientation (SPO) of the orbicules (Supplementary material, Annex 1), constrictional flow or flattening deformation did not operate during the crystallization process, although the orbicules interacted in the orbicular magma as is evidenced by the plasticity of their mutual contacts. A simple inmiscibility between two liquids or silicate gels does not explain why the radial gabbroic assemblage is rooted around the cold germs. The crystallization-induced fractionation accounts for the internal composition of the orbicules.

Crystallization proceeded differently with time. Higher undercooling rates (columnar crystallization) are observed in the gabbroic sub-system where the solidus temperature is higher, which involves a great undercooling (Lofgren, 1974; Spillar and Dolejs, 2013). Conversely, in the granodioritic sub-system, equiaxial crystallization was promoted by low relative crystallization rates due to solidus temperatures lower than in the inner shell. Besides, dispersed nuclei could have grown in the granodioritic sub-system during the initial orbicular shell growth, causing the shift from orbicular to normal crystallization (Fenn, 1977; Grosse et al., 2010; Swanson, 1977; Vernon, 1985). Therefore, the sudden "explosive" crystallization in the inner shell should have occurred first, triggering fractionation of the gabbroic sub-system. According to the Hbl-Pl equilibrium temperatures calculated in the orbicular matrix and this crystallization sequence, this process took place at above 875 °C. The rest of the crystallization process evolved

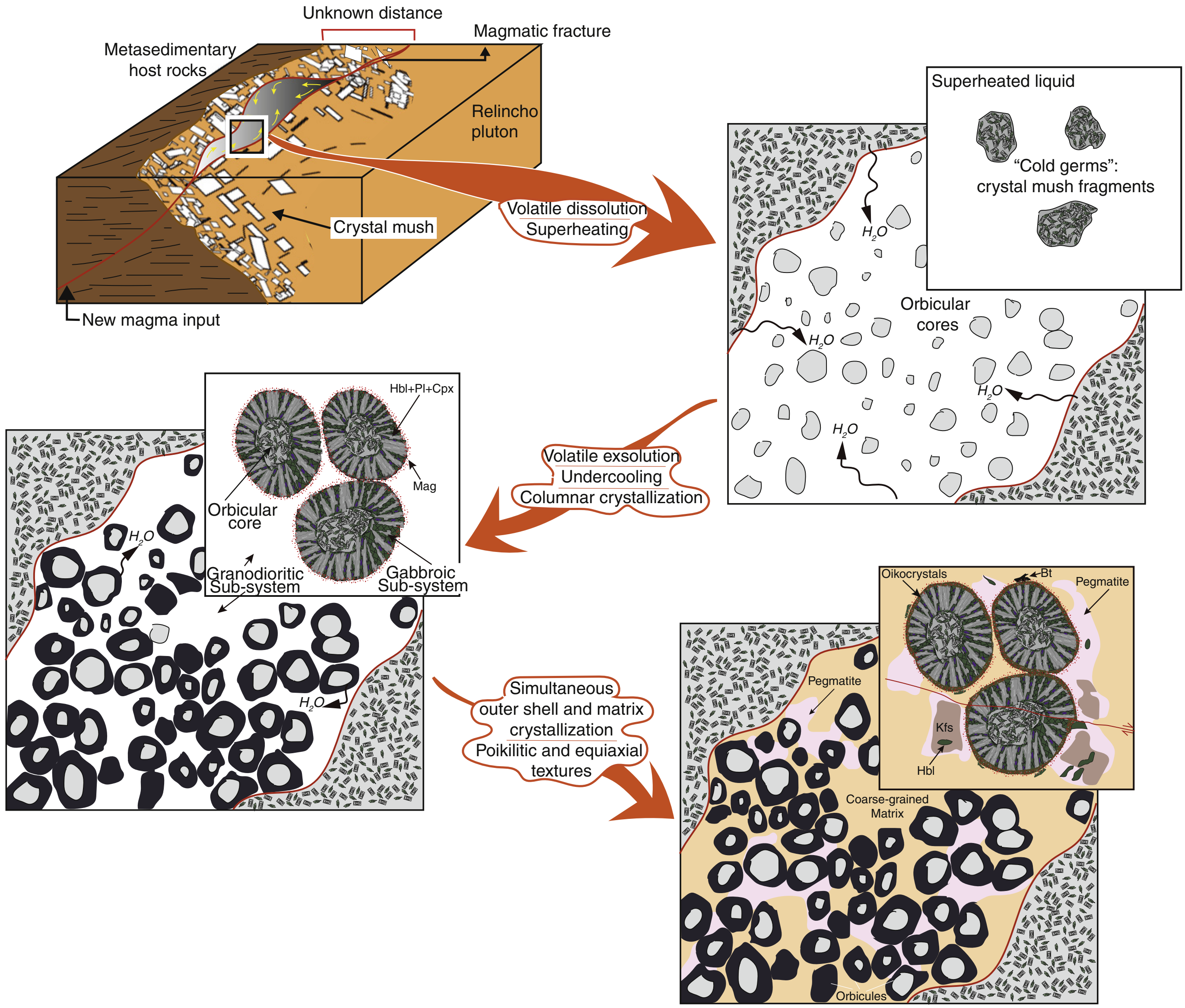

Fig. 11. Interpretative sketch of the formation of the orbicular granitoid of Caldera.

later in the outer shell and the matrix, as suggested by the poikilitic textures observed in both sides of the orbicule contact (Fig. 3), and under conditions close to the solidus of both sub-systems (shell and matrix). Nevertheless, the rapidity of the crystallization in the orbicular body is emphasized by the different crystallographic orientation of interstitial quartz crystals in the inner shell and the outer shell-matrix contact, which mimic the orthogonal arrangement of large crystals in both zones. Quartz CPO evidences that the undercooling conditions were leading during the entire crystallization process of the orbicules. The H_2O-rich residual liquid expelled during the orbicular shell crystallization in the gabbroic subsystem was mingled with the partially crystallized matrix magma, generating the pegmatitic domains with large Kfs megacrysts (Fig. 11). The quickness of the entire process explains why the orbicules fit to the shape of the contacts and that Kfs megacrystals are plastically deformed where they were trapped between orbicules (Fig. 2).

8. Conclusions

The orbicular granitoid of Caldera (Chile) is a remarkable example of radial orbicular textures. Its outcrop, confined to a few square meters ($375\ m^2$) next to the Pacific Ocean and emplaced in the Lower Jurassic Relincho pluton, is recognized as a Nature Sanctuary in Chile and visited by tourists and curious. A detailed geochemical and textural study has been used to propose a complex model of orbicule generation considering processes of super-heating, undercooling and fractionation, together with the crucial effect of the injection of water into the orbicular magma and subsequent volatile exsolution. The core of the orbicules shows equiaxial textures and dioritic to tonalitic compositions, similar to those of the host rock. In contrast, the orbicule shell presents an inner zone with radial, feathery textures, and an outer zone with large oikocrystals arranged parallel to the external contact of the orbicule. Geochemically, the orbicule shell is a gabbro, which contrasts with the granodioritic composition of the matrix showing holocrystalline equiaxial to pegmatitic textures. The crystallographic orientation of interstitial quartz crystals matches the texture of the large crystals of Pl and Hbl in the shell and matrix, evidencing rapid crystallization processes. Thermobarometry yielded pressure values in the range 3–4 kbar, and temperature conditions of 835–875 °C for the core and 875–900 °C for the matrix, which impose the maximum starting and minimum final temperature during the orbicule crystallization process, respectively. Relative distribution of major, highly compatible and large-ion incompatible elements in the orbicule shell and matrix can be explained by a process of fractional crystallization from a parental dioritic magma giving rise to the gabbroic shell and the granodioritic matrix. On the other hand, orbicule and matrix show similar contents of REE, Sr, and Y, which is explained as a consequence of crystal-liquid disequilibrium and heterogeneous crystallization related to undercooling conditions. Crystallization modeling with MELTS supports the observed geochemical features and highlights the importance of a process of sudden water decrease or exsolution during the first stages of orbicule crystallization. The proposed conceptual model for the orbicular body of Caldera considers emplacement of a dioritic magma batch within the crystallization front of a host magma body. The host magma pluton provided the cores of the future orbicules and a significant volume of H_2O-rich residual liquids that fluxed from the host magma mush into the low-pressure, newly intruding magma batch. The superheated magma evolved exsolving the volatile excess to reach equilibrium with the emplacement conditions, and the consequent volatile loss and undercooling gave place to super-fast crystallization (around 1–5 mm/day) of the shell crystals around the cores. In turn, this process of heterogeneous crystallization led to rapid fractionation of major and some trace elements between a gabbroic solid assemblage (orbicule) and a granodioritic melt (matrix) and unfractionated distributions of REE, Sr or Y because their distribution coefficients approached unity. Final crystallization in the orbicule-matrix contact took place near the solidus originating large Hbl and Bt oikocrystals, which are disposed orthogonal to the radiate structure of the shell, and equiaxial textures in the orbicular matrix, with the H_2O-rich residual liquid generating pegmatitic domains. Although this model is specifically intended to explain the orbicular granitoid of Caldera, we propose that the suggested processes could serve as a reference framework to understand other similar cases of orbicular textures around the world.

Supplementary data to this article can be found online at http://dx.doi.org/10.1016/j.lithos.2017.04.017.

Acknowledgements

Our group acknowledges and recognizes Aguirre and collaborators for introducing us to the fascinating world of the orbicular granitoid of Caldera through their pioneer manuscript in 1976.

The idea of this work was developed during the pre-graduated Thesis proposal of Ítalo Constanzo, carried out at the Department of Geology of the University of Atacama. We are grateful for constructive colleague reviews by Gustavo Miranda and Wolfgang Griem, both of whom improved the manuscript. C. R. is grateful for her postdoctoral contract from the University of Huelva (under the Estrategia Politíca Científica de la UHU 2016/2017). We would like to sincerely thank the editor and the reviewers (J.L. Vigneresse and an anonymous referee) of LITHOS for their thorough corrections of the first draft of this manuscript.

The work was funded with DIUDA 2014-22273 project of the University of Atacama with the fund support of FONDECYT Project N° 11140722 of CONICYT.

References

Abdallah, N., Liégeois, J., De Waele, B., Fezaa, N., Ouabadi, A., 2007. The Temaguessine Fe-cordierite orbicular granite (Central Hoggar, Algeria): U-Pb SHRIMP age, petrology, origin and geodynamical consequences for the late Pan-African magmatism of the Tuareg shield. Journal of African Earth Sciences 49, 153–178.

Aguirre, L., Hervé, F., Del Campo, M., 1976. An orbicular tonalite from caldera, Chile. Journal of the Faculty of Science, Hokkaido University 17-2, 231–259.

Anderson, J.L., Smith, D.R., 1995. The effect of temperature and oxygen fugacity on Al-in-hornblende barometry. American Mineralogist 80, 549–559.

Arzilli, F., Mancini, L., Voltolini, M., Cicconi, M.R., Mohammadi, S., Giuli, G., Mainprice, D., Paris, E., Barou, F., Carroll, M.R., 2015. Near-liquidus growth of feldspar spherulites in trachytic melts: 3D morphologies and implications in crystallization mechanisms. Lithos 216-217, 93–105.

Ballhaus, C., Fonseca, R.O.C., Münker, C., Kirchenbaur, M., Zirner, A., 2015. Spheroidal textures in igneous rocks — textural consequences of H_2O saturation in basaltic melts. Geochimica et Cosmochimica Acta 167, 241–252.

Barrière, M., 1972. Le gabbro orbiculairedes Alharisses (massif de Néouvielle, Pyrénées francaises). Bulletin de la Société Française de Minéralogie et de Crystallographie 95, 495–506.

Barrière, M., Chauris, L., Cotten, J., 1971. Premières données sur un faciès orbiculaire dans le massif granitique de l'Aber-Ildut (Finistère, France). Bulletin de la Société Française de Minéralogie et de Crystallographie 94, 402–410.

Bea, F., Pereira, M.D., Stroh, A., 1994. Mineral/leucosome trace-element partitioning in a peraluminous migmatite (a laser ablation-ICP-MS study). Chemical Geology 117 (1–4), 291–312.

Bell, C.M., 1982. The lower paleozoic metasedimentary basament of the coastal ranges of Chile between 25°30′ and 27°S. Revista Geológica de Chile 17, 21–29.

Brandon, A.D., Draper, D.S., 1996. Constraints on the origin of the oxidation state of mantle overlying subduction zones: an example from Simcoe, Washington, USA. Geochimica et Cosmochimica Acta 60, 1739–1749.

Brook, M., Pankhurst, R., Sheperd, T., Spiro, B., Snelling, N., Swainbank, I., 1986. Andean Geochronology and Metallogenesis. Open File ReportOverseas Development Administration, London (83 pp.).

Browne, D.J., 2002. Modelling Columnar and Equiaxed Growth. (Thesis). Department of Materials. University of Oxford (227 pp.).

Carmichael, I.S.E., 1991. The redox states of basic and silicic magmas: a reflection of their source regions? Contributions to Mineralogy and Petrology 106, 129–141.

Carvalho, D.B., Moreira, A.L., Moutinho, D.J., Filho, J.M., Rocha, O.L., Spinelli, J.E., 2013. The columnar to equiaxed transition of horizontal unsteady-state directionally solidified Al–Si alloys. Materials Research 17 (2), 498–510.

Castro, A., 2013. Tonalite-granodiorite suites as cotectic systems: a review of experimental studies with application to granitoid petrogenesis. Earth Science Reviews 124, 68–95.

Castro, A., Martino, R., Vujovich, G., Otamendi, J., Pinotti, L., D'Eramo, F., Tibaldi, A., Viñao, A., 2008. Top-down structures of mafic enclaves within the Valle Fértil magmatic complex (Early Ordovician, San Juan, Argentina). Geologica Acta 6, 217–229.

Charrier, R., Pinto, L., Rodríguez, M.P., 2007. Tectonostratigraphic evolution of the Andean orogen in Chile. In: Moreno, T., Gibbons, W. (Eds.), The Geology of Chile. the Geological Society, London, pp. 21–114.

Chauris, L., Hallégouët, B., Riva, N., 1989. Données préliminaires sur un faciès orbiculaire dans le granite rouge de Ploumanac'h (Massif armoricain). Comptes Rendus de l'Académie des Sciences Paris 309, 59–62.

Couturié, J.P., 1973. Un nouveau gisement de granite orbiculaire dans le Massif Central francais: le granite du Signal de Randon (Lozère). Contributions to Mineralogy and Petrology 42, 305–312.

Dallmeyer, R.D., Brown, M., Grocott, J., Taylor, G.K., Treloar, P.J., 1996. Mesozoic magmatic and tectonics events within the Andean Plate boundary zone, 26°–27°30′S, North Chile: constraints from $^{40}Ar/^{39}Ar$ Mineral ages. Journal of Geology 104, 19–40.

Decrite, S., Gasquet, D., Marignac, C., 2002. Genesis of orbicular granitic rocks from the Ploumanac'h Plutonic Complex (Brittany, France): petrographical, mineralogical and geochemical constraints. European Journal of Mineralogy 14, 715-31.

Durant, D.G., Fowler, A.D., 2002. Origin of reverse zoning in branching orthopyroxene and acicular plagioclase in orbicular diorite, Fisher Lake, California. Mineralogical Magazine 66, 1003-19.

Elliston, J.N., 1984. Orbicules: an indication of the crystallization of hydrosilicates, I. Earth Science Reviews 20, 265–344.

Elliston, J.N., 1985. Rapakivi texture: an indication of the crystallization of hydrosilicates, II. Earth-Science Reviews 22, 1–92.

Enz, R., Kudo, A., Brookins, D.G., 1979. Igneous origin of the orbicular rocks of the Sandia Mountains, New Mexico. Bulletin of the Geological Society of America 90, 138–140.

Eskola, P., 1938. On the esboitic crystallization of orbicular rocks. Journal of Geology 46, 448-85.

Farrar, E., Clark, A., Haynes, J., Quirt, G., Conn, H., Zentilli, M., 1970. K-Ar evidence for the post-Paleozoic migration of granitic intrusion foci in the Andes of northern Chile. Earth and Planetary Science Letters 10, 60–66.

Fenn, P.M., 1972. Nucleation and growth of alkali feldspars from synthetic melts [abs.]. Transactions of the American Geophysical Union 53, 1127.

Fenn, P.M., 1977. The nucleation and growth of alkali feldspars from hydrous melts. Canadian Mineralogist 15, 135–161.

Fernández, C., Castro, A., 1999. Brittle behaviour of granitic magma: the example of Puente del congosto, Iberian massif, Spain. Geological Society, London, Special Publications 168, 191–206.

Frost, B.R., Barnes, C.G., Collins, W.J., Arculus, R.J., Ellis, D.J., Frost, C.D., 2001. A geochemical classification for granitic rocks. Journal of Petrology 42, 2033–2048.

Fuentes, P., Díaz-Alvarado, J., Fernández, C., Díaz-Azpíroz, M., Rodríguez, N., 2016. Structural analysis and shape-preferred orientation determination of the mélange facies in the Chañaral mélange, Las Tórtolas Formation, Coastal Cordillera, northern Chile. Journal of South American Earth Sciences 67, 40–56.

Ghiorso, M.S., Sack, R.O., 1995. Chemical mass transfer in magmatic processes. IV. A revised and internally consistent thermodynamic model for the interpolation and extrapolation of liquid-solid equilibria in magmatic systems at elevated temperatures and pressures. Contributions to Mineralogy and Petrology 119, 197–212.

Godoy, E., Lara, P.L., 1999. Hoja Puerto Flamenco, Región de Atacama. Servicio Nacional de Geología y Minería. Mapas Geológicos no. 15, 1 mapa escala 1:100.000, Santiago.

Goodspeed, G.E., 1942. Orbicular rocks from Buffalo Hump, Idaho. American Mineralogist 27, 37–47.

Grosse, P., Toselli, A., Rossi, J., 2010. Petrology and geochemistry of the orbicular granitoid of Sierra de Velasco (NW Argentina) and implications for the origin of orbicular rocks. Geological Magazine 147 (3), 451–468.

Gualda, G.A.R., Ghiorso, M.S., Lemons, R.V., Carley, T.L., 2012. Rhyolite-MELTS: a modified calibration of MELTS optimized for silica-rich, fluid-bearing magmatic systems. Journal of Petrology 53, 875–890.

Hammer, J.E., Rutherford, M.J., 2002. An experimental study of the kinetics of decompression-induced crystallization in silicic melt. Journal of Geophysical Research 107, 8–24.

Henderson, P., 1986. Inorganic Geochemistry. Pergamon Press, Oxford (353 pp.).

Holland, T., Blundy, J., 1994. Non-ideal interactions in calcic amphiboles and their bearing on amphibole-plagioclase thermometry. Contributions to Mineralogy and Petrology 116, 433–447.

Iezzi, G., Mollo, S., Ventura, G., 2009. Solidification behaviour of natural silicate melts and volcanological implications. In: Lewis, N., Moretti, A. (Eds.), Volcanoes: Formation, Eruptions and Modelling. Nova Publishers, New York, pp. 127–151.

Jahns, R.H., Burnham, C.W., 1969. Experimental studies of pegmatite genesis. I. A model for the derivation and crystallization of granitic pegmatites. Economic Geology 64, 843–864.

Johannes, W., Holtz, F., 1996. Petrogenesis and Experimental Petrology of Granitic Rocks. Springer, Berlin.

Keith, H.D., Padden Jr., F.J., 1963. A phenomenological theory of spherulitic crystallization. Journal of Applied Physics 34, 2409–2421.

Kelemen, P.B., Hanghoj, K., Greene, A.R., 2003. One view of the geochemistry of subduction-related magmatic arcs, with emphasis on primitive andesite and lower crust. In: Rudnick, R.L. (Ed.), The Crust. Elsevier, Amsterdam, pp. 593–659.

Kennan, P., Lorenc, M., 2008. Orbicular granite near Jelenia Góra in southwestern Poland: the first outcrops? Mineralogia 39 (3–4), 79–85.

Kretz, R., 1983. Symbols for rock-forming minerals. American Mineralogist 68, 277–279.

Lahti, S., 2005. Orbicular Rocks in Finland. Geological Survey of Finland, Espoo, p. 177.

Launeau, P., Robin, P.-Y.F., 2005. Determination of fabric and strain ellipsoids from measured sectional ellipses — implementation and applications. Journal of Structural Geology 27, 2223–2233.

Le Bas, M.J., Le Maitre, R.W., Streckeisen, A., Zanettin, B., 1986. A chemical classification of volcanic rocks based on the total alkali-silica diagram. Journal of Petrology 27, 745–750.

Lee, C.T.A., Morton, D.M., 2015. High silica granites: terminal porosity and crystal settling in shallow magma chambers. Earth and Planetary Science Letters 409, 23–31.

Leveson, D.J., 1966. Orbicular rocks: a review. Bulletin of the Geological Society of America 77, 409-26.

Lindh, A., Näsström, H., 2006. Crystallization of orbicular rocks exemplified by the Slättemossa occurrence, southeastern Sweden. Geological Magazine 143, 713–722.

Lofgren, G.E., 1974. An experimental study of plagioclase crystal morphology: isothermal crystallization. American Journal of Science 274, 243–273.

London, D., 1992. The applicationof experimentalpetrology to the genesis and crystallization of granitic pegmatites. The Canadian Mineralogist 30, 499–540.

London, D., 2009. The origin of primary textures in granitic pegmatites. The Canadian Mineralogist 47, 697–724.

London, D., Morgan, G.B., Hervig, R.L., 1989. Vapor undersaturated experiments with Macusani glass + H_2O at 200 MPa, and the internal differentiation of granitic pegmatites. Contributions to Mineralogy and Petrology 102, 1–17.

Marsh, B.D., 1996. Solidification fronts and magmatic evolution. Mineralogical Magazine 60, 5–40.

Meyer, H.P., Altherr, R., 1991. A model for the genesis of orbicular granitoid rocks. Terra Abstracts 3, 426.

Moore, J.G., Lockwood, J.P., 1973. Origin of comb layering and orbicular structure, Sierra Nevada batholith, California. Bulletin of the Geological Society of America 84, 1–20.

Mpodozis, C., Ramos, V.A., 2008. Tectónica Jurásica en Argentina y Chile: extensión, subducción oblicua, rifting, deriva y colisiones? Revista de la Asociación Geológica Argentina 63 (4), 481–497.

Nakamura, N., 1974. Determination of REE, Ba, Fe, Mg, Na and K in carbonaceous and ordinary chondrites. Geochimica et Cosmochimica Acta 38, 757–775.

Naney, M.T., 1983. Phase equilibria of rock forming ferromagnesian silicates in granitic systems. American Journal of Science 283, 993–1033.

Ort, M., 1992. Orbicular volcanic rocks of Cerro Panizos: their origin and implications for orb formation. Bulletin of the Geological Society of America 104, 1048–1058.

Owen, J., 1991. Significance of epidote in orbicular diorite from the Grenville Front zone, eastern Labrador. Mineralogical Magazine 55, 173–181.

Palmer, D.F., Bradley, J., Prebble, W.M., 1967. Orbicular granodiorite from Taylor Valley, South Victoria Land, Antartica. Geological Society of America Bulletin 78, 1423–1428.

Parkinson, I.J., Arculus, R.J., 1999. The redox state of subduction zones: insights from arc-peridotites. Chemical Geology 160, 409–423.

Piboule, M., Soden, L., Amossé, J., Briand, B., 1989. Le massif basique de Loreto di Tallano (Corse du Sud): mise en évidence du contrôle de la surfusion adiabatique dans la genèse des faciès orbiculaires. Comptes Rendus de l'Académie des Sciences Paris 309, 713–718.

Robin, P.-Y.F., 2002. Determination of fabric and strain ellipsoids from measured sectional ellipses — theory. Journal of Structural Geology 24, 531–544.

Rodríguez, N., Díaz-Alvarado, J., Rodríguez, C., Riveros, K., Fuentes, P., 2016. Petrology, geochemistry and thermobarometry of the northern area of the Flamenco pluton, Coastal Range batholith, northern Chile. A thermal approach to the emplacement processes in the Jurassic Andean batholiths. Journal of South American Earth Sciences 67, 122–139.

Rollinson, H.R., 1993. Using Geochemical Data: Evaluation, Presentation and Interpretation. Longman Scientific and Technical, Harlow, Essex, England (352 pp.).

Rubin, A.M., 1993. Dikes vs diapirs in viscoelastic rocks. Earth and Planetary Science Letters 117, 653–670.

Schmidt, M.W., 1992. Amphibole composition in tonalite as a function of pressure: an experimental calibration of the Al-in-hornblende barometer. Contributions to Mineralogy and Petrology 110, 304–310.

Sederholm, J., 1928. On orbicular granites, spotted and nodular granites, etc., and the rapakivi texture. Bulletin de la Commission Géologique de Finlande 83, 1–105.

Sinclair, W., Richardson, J., 1992. Quartztourmaline orbicules in the Seagull batholith, Yukon Territory. Canadian Mineralogist 30, 923–935.

Spillar, V., Dolejs, D., 2013. Calculation of time-dependent nucleation and growth rates from quantitativetextural data: inversion of crystal size distribution. Journal of Petrology 54, 913–931.

Swanson, S.E., 1977. Relation of nucleation and crystal growth rate to the development of granite textures. American Mineralogist 62, 966-78.

Symes, R., Bevan, J., Qasim, J., 1987. The nature and origin of orbicular rocks from near Deshai, Swat Kohistan, Pakistan. Mineralogical Magazine 51, 635–647.

Tagiri, M., Oba, T., Fujinawa, A., 2007. Radial cordierite-bearing orbicular granite formed from the melting of Pelitic Hornfels in granitic magma, Tsukuba Montains, Japan. Journal of Mineralogical and Petrological Sciences 102, 127–136.

Thévoz, P., 1998. Modelling of columnar and equiaxed solidification. Solidification Course 1998, May 10–15, Savannah, Georgia, USA. CALCOM SA (47 pp.).

Vernon, R.H., 1985. Possible role of superheated magma in the formation of orbicular granitoids. Geology 13, 843-45.

Vigneresse, J.L., 2014. Textures and melt-crystal-gas interactions in granites. Geoscience Frontiers 6, 635–663.

Waters, L.E., Andrews, B.J., Lange, R.A., 2015. Rapid crystallization of plagioclase phenocrysts in silicic melts during fluid-saturated ascent: phase equilibrium and decompression experiments. Journal of Petrology 56, 981–1006.

Wilson, M., 1989. Igneous Petrogenesis. A Global Tectonic Approach. Unwin Hyman, London (466 pp.).

Winkler, H.G.F., Lindemann, W., 1972. The system Qz—Or—An—H_2O in the granite system Qz—Or—Ab—An—H_2O. Applications to granite magma formation. Neues Jahrbuch der Mineralogie, Monatschefte 49–61.